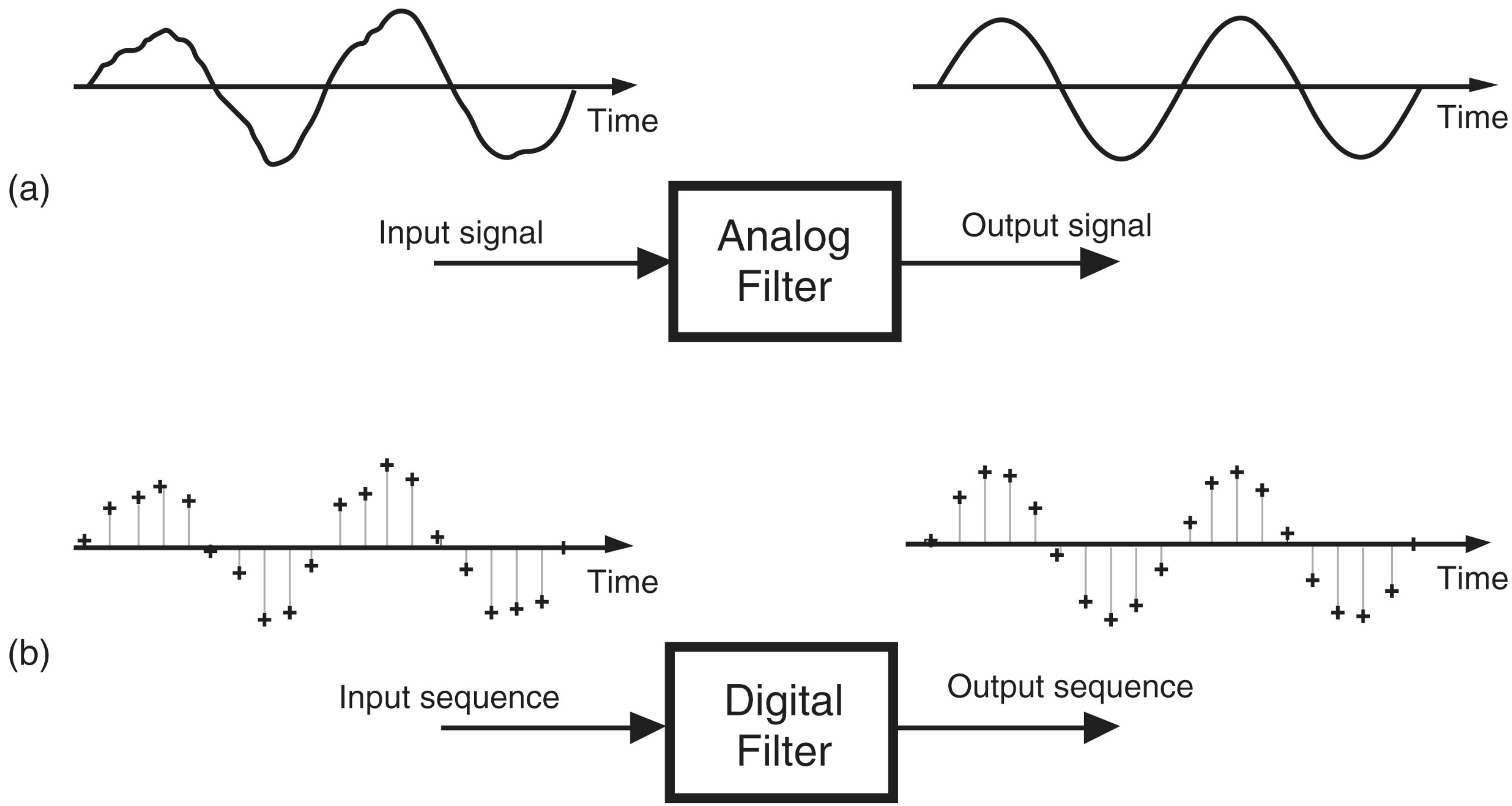

Figure 5–1 Filters: (a) an analog filter with a noisy tone input and a reduced-noise tone output; (b) the digital equivalent of the analog filter.

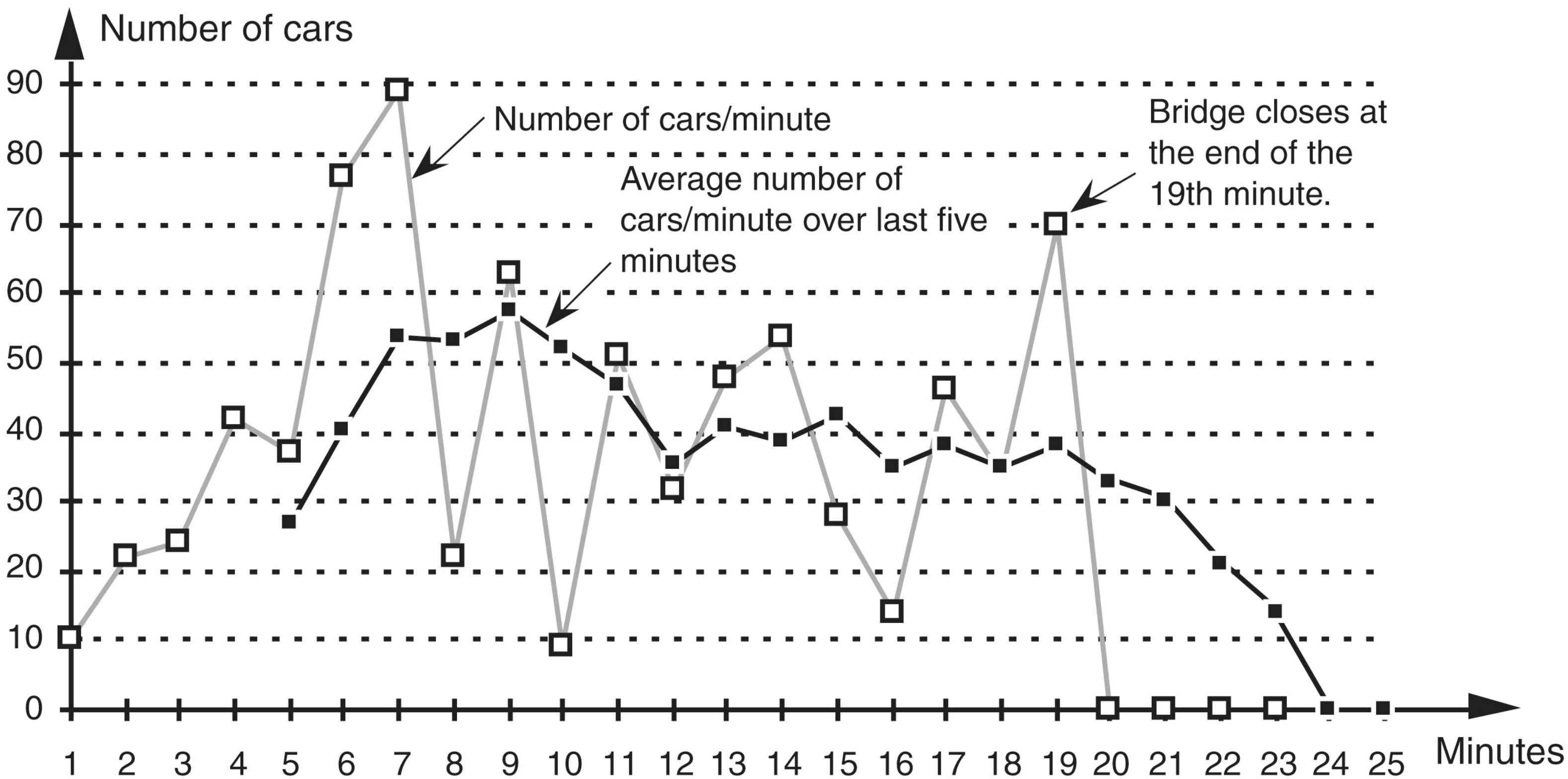

Figure 5–2 Averaging the number of cars/minute. The dashed line shows the individual cars/minute, and the solid line is the number of cars/minute averaged over the last five minutes.

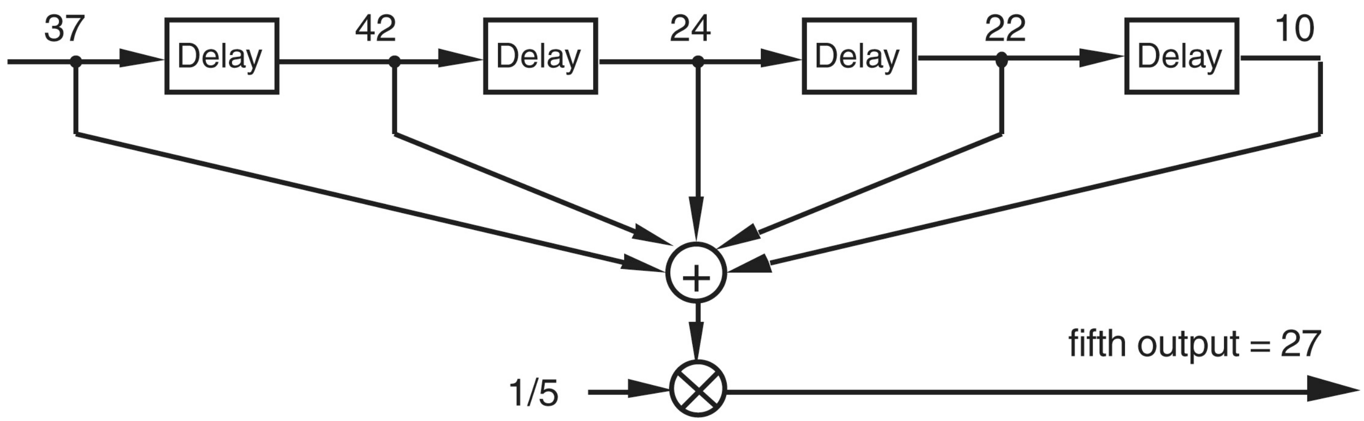

Figure 5–3 Averaging filter block diagram when the fifth input sample value, 37, is applied.

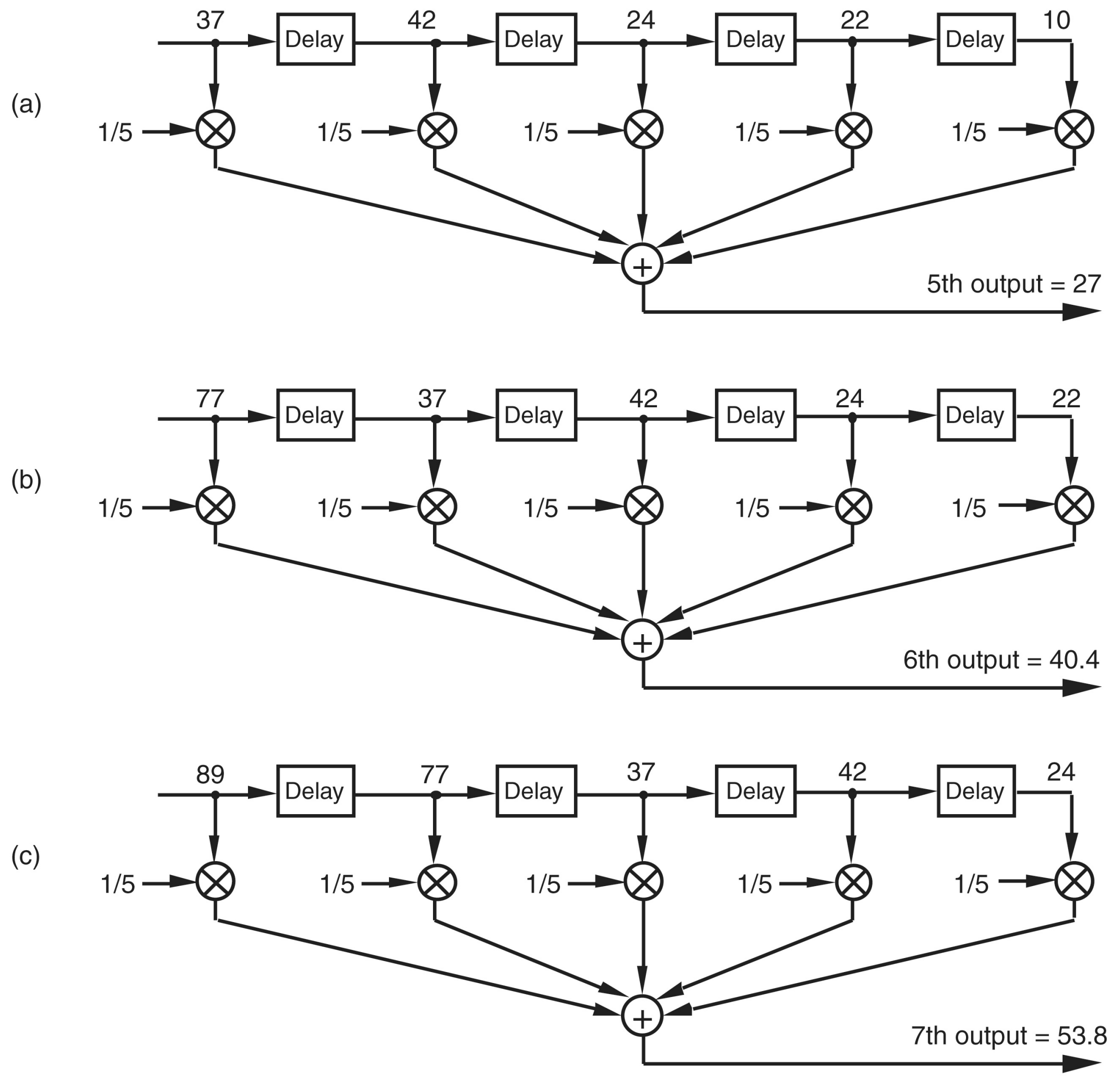

Figure 5–4 Alternate averaging filter structure: (a) input values used for the fifth output value; (b) input values used for the sixth output value; (c) input values used for the seventh output value.

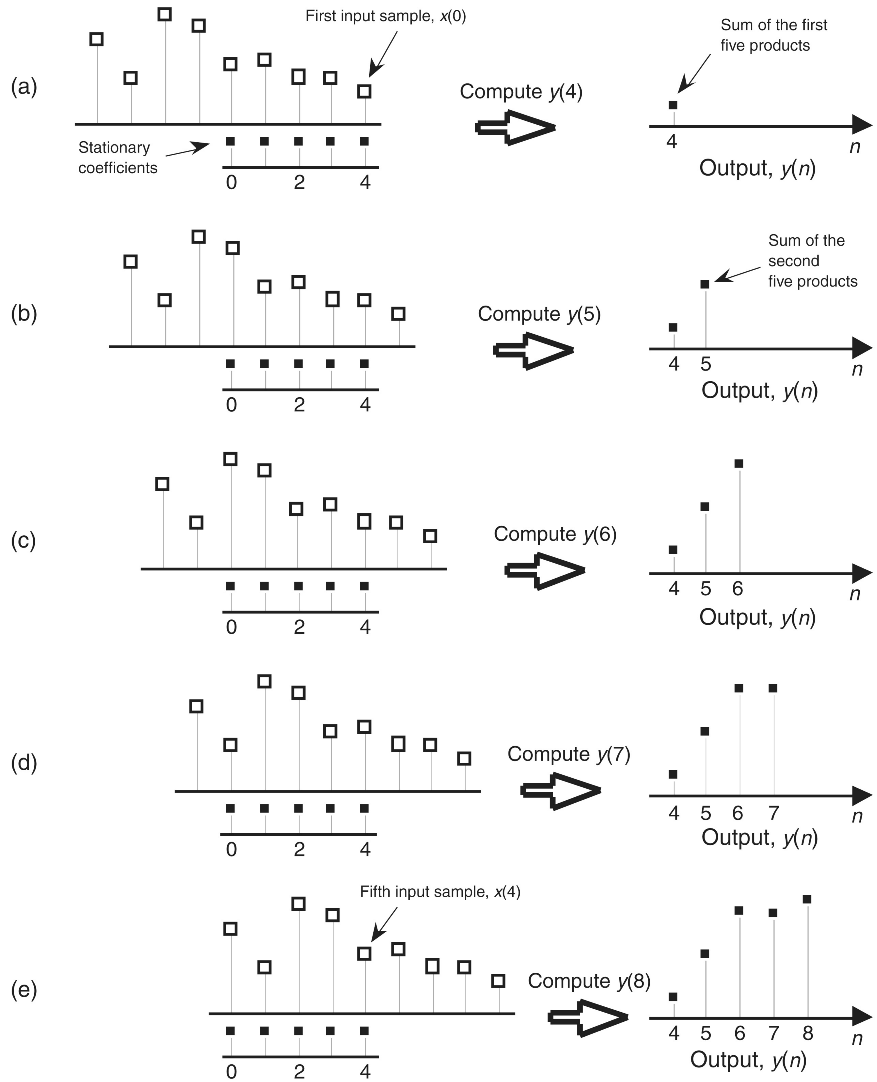

Figure 5–5 Averaging filter convolution: (a) first five input samples aligned with the stationary filter coefficients, index $n = 4$; (b) input samples shift to the right and index $n = 5$; (c) index $n = 6$; (d) index $n = 7$; (e) index $n = 8$.

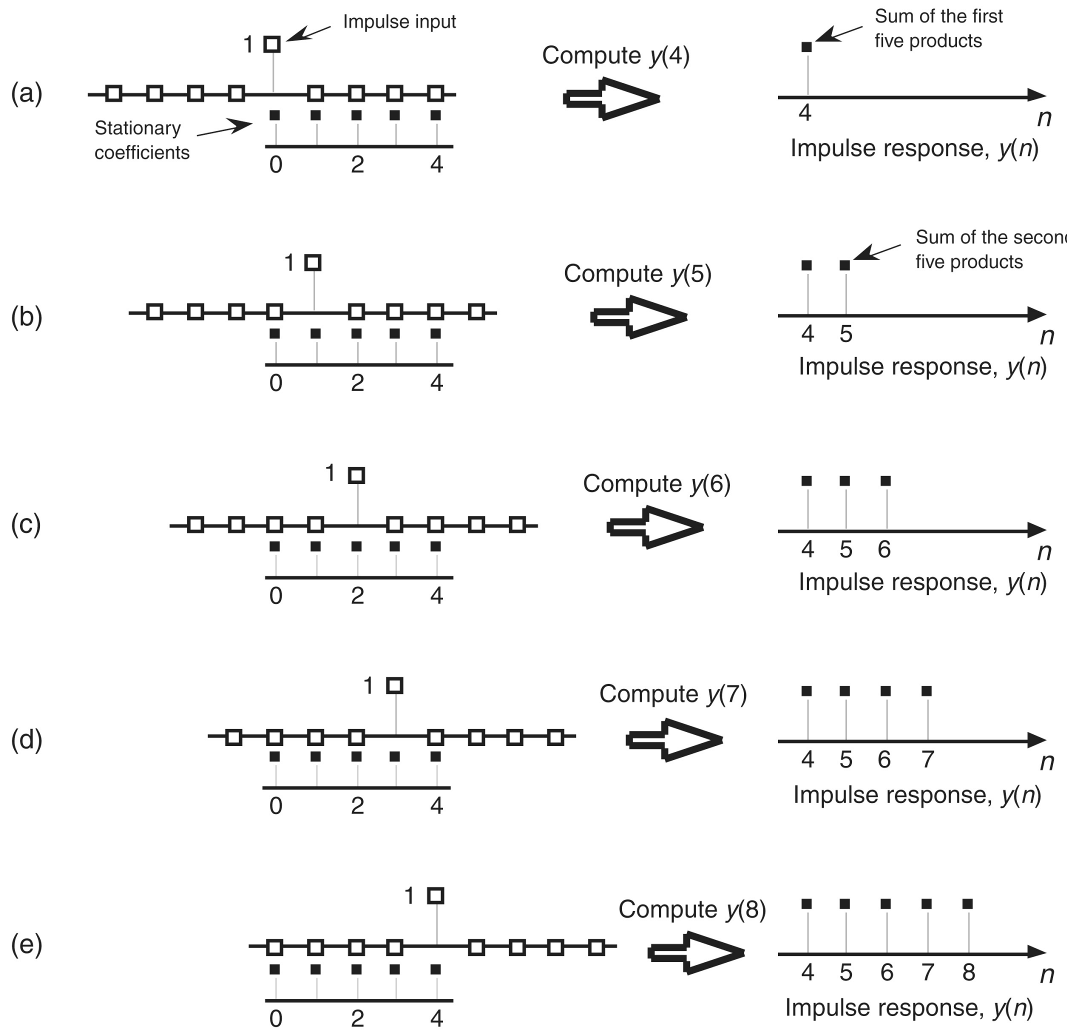

Figure 5–6 Convolution of filter coefficients and an input impulse to obtain the filter's output impulse response: (a) impulse sample aligned with the first filter coefficient, index $n = 4$; (b) impulse sample shifts to the right and index $n = 5$; (c) index $n = 6$; (d) index $n = 7$; (e) index $n = 8$.

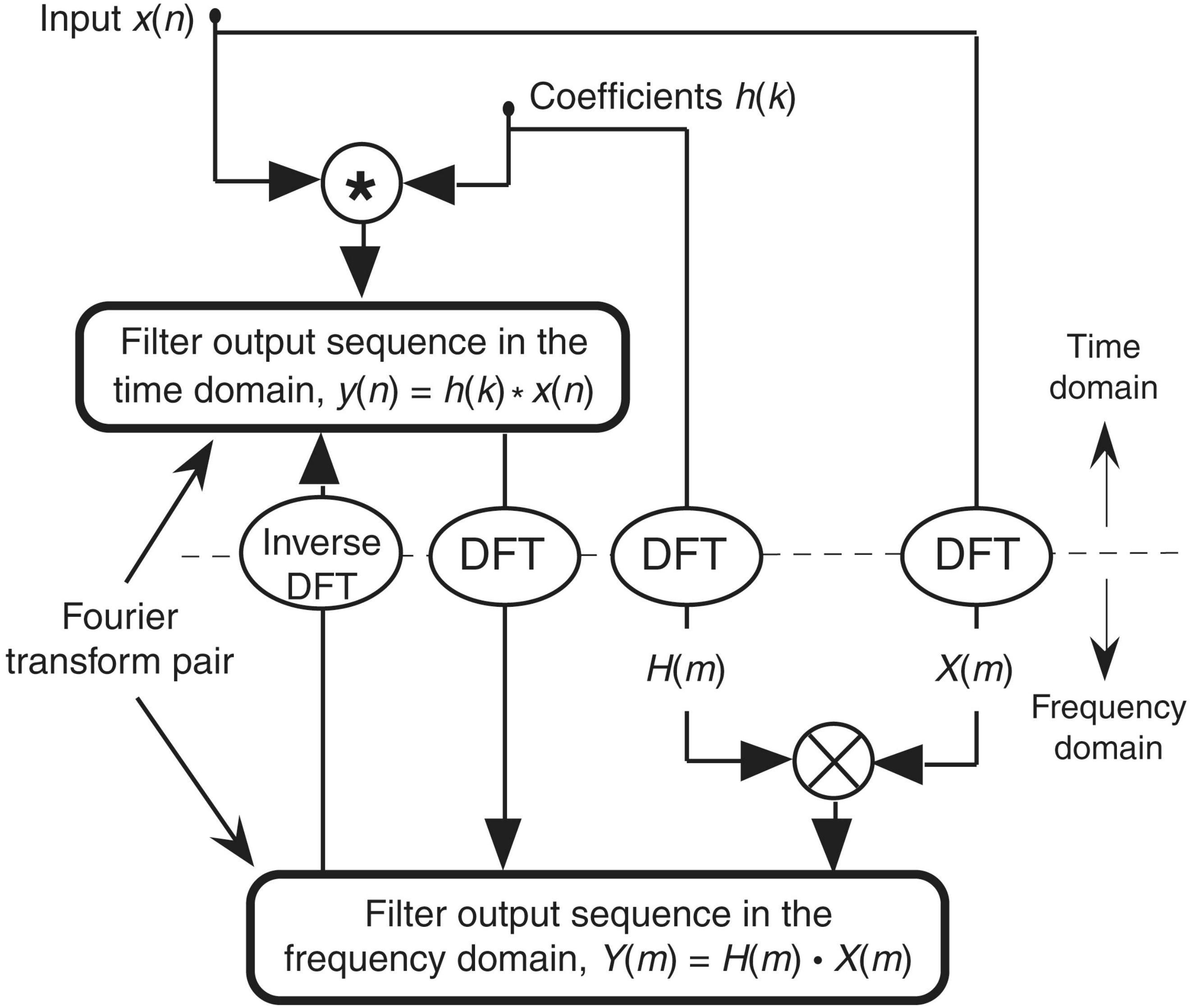

Figure 5–7 Relationships of convolution as applied to FIR digital filters.

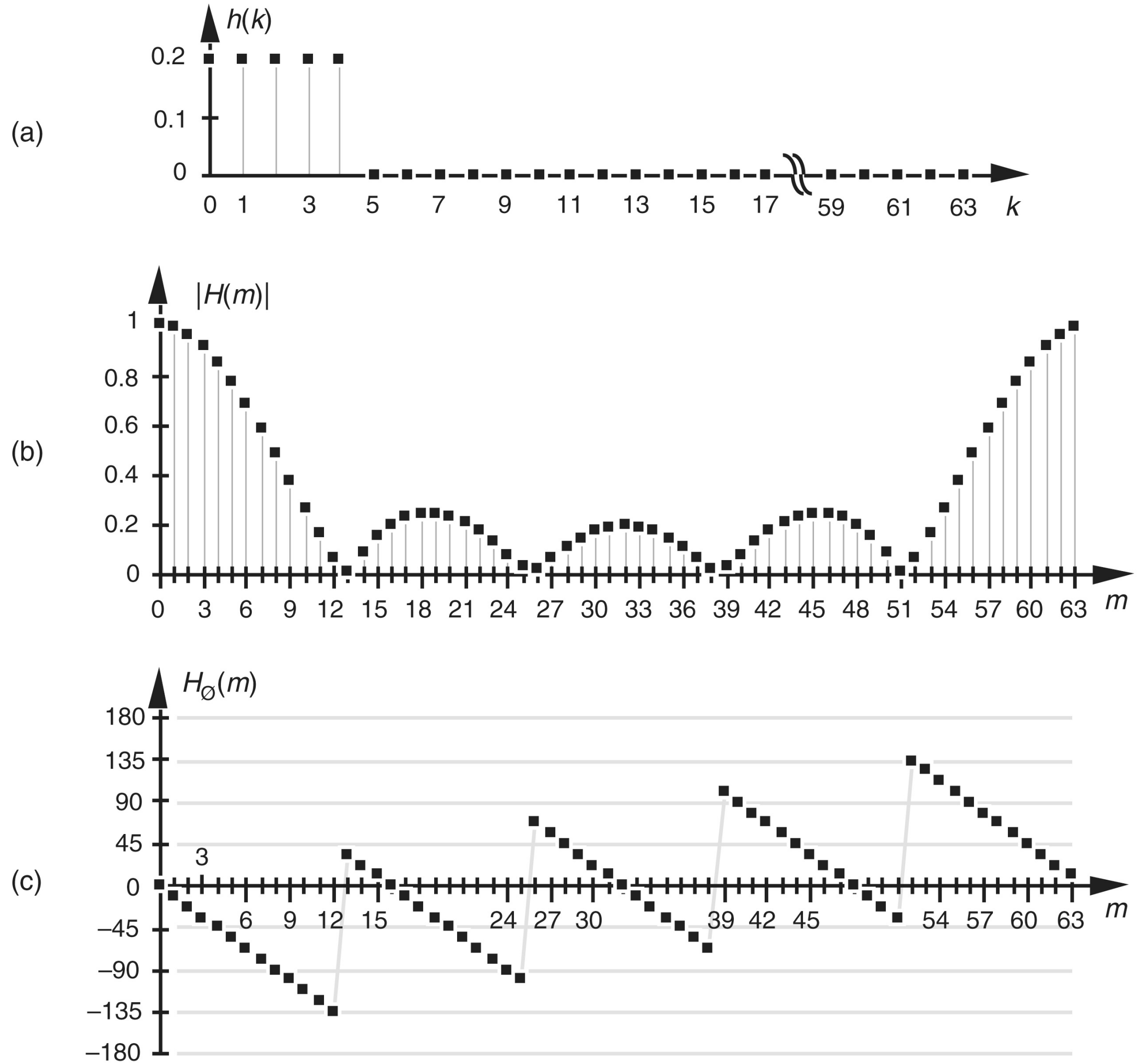

Figure 5–8 Averaging FIR filter: (a) filter coefficient sequence $h(k)$ with appended zeros; (b) normalized discrete frequency magnitude response $|H(m)|$ of the $h(k)$ filter coefficients; (c) phase-angle response of $H(m)$ in degrees.

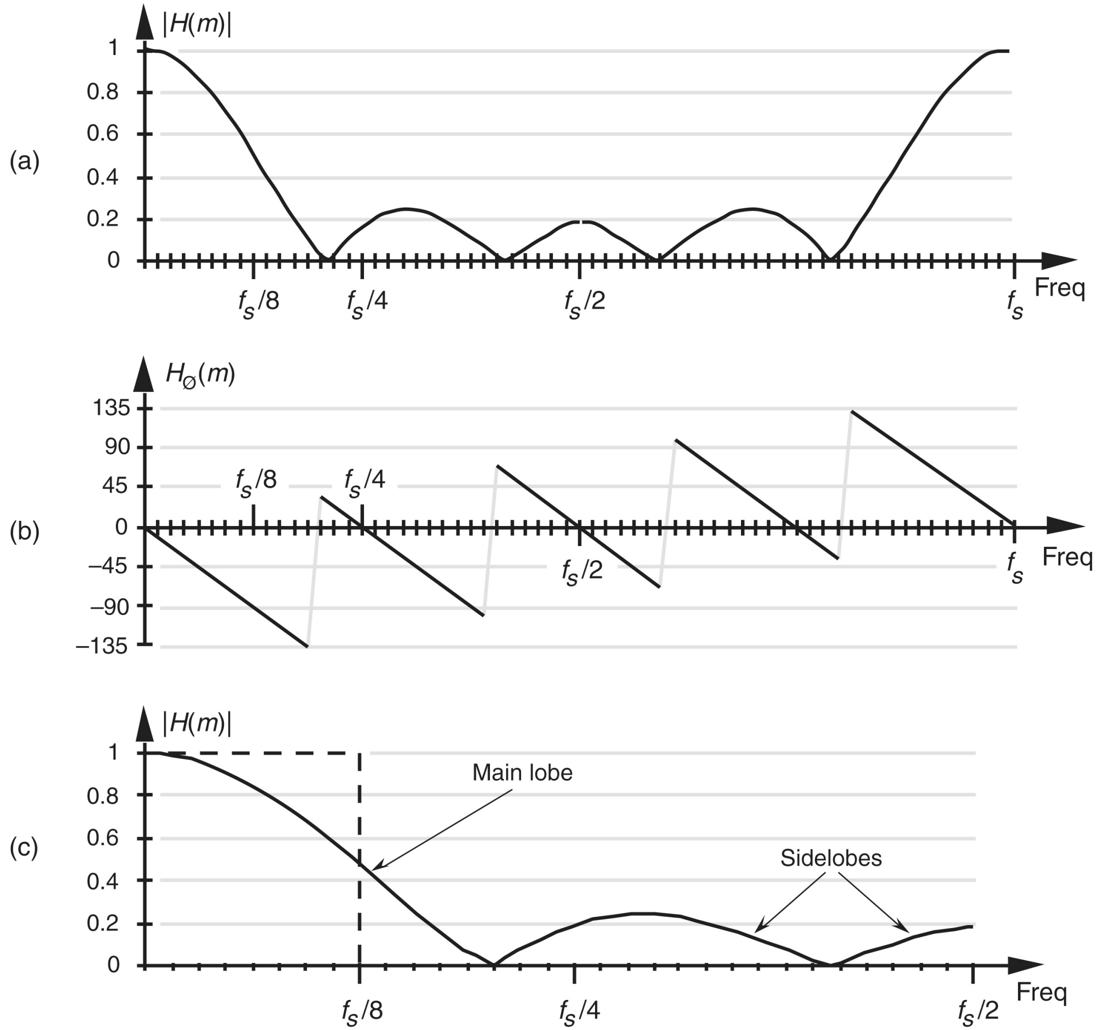

Figure 5–9 Averaging FIR filter frequency response shown as continuous curves: (a) normalized frequency magnitude response, $|H(m)|$; (b) phase-angle response of $H(m)$ in degrees; (c) the filter's magnitude response between zero Hz and half the sample rate, $f_s/2$ Hz.

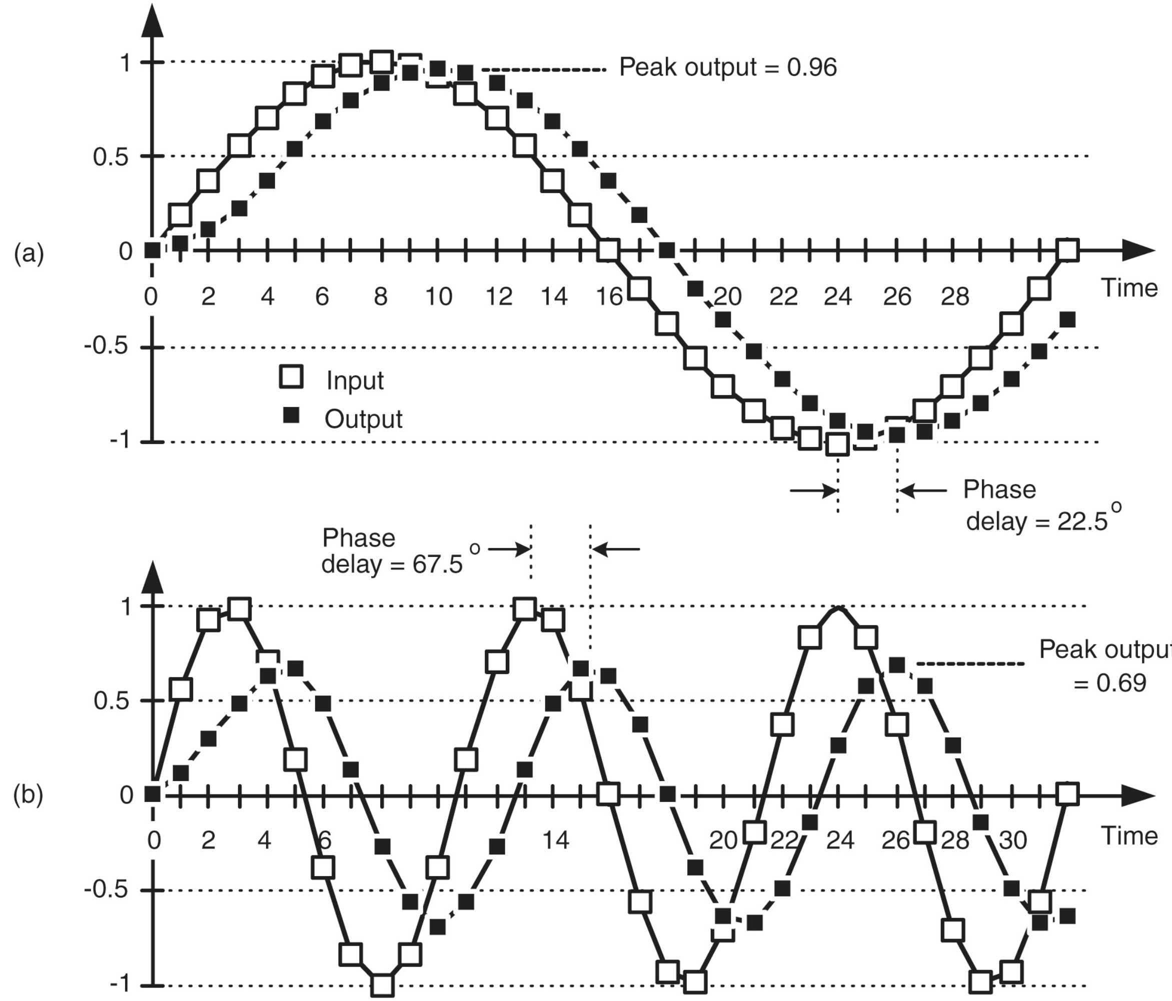

Figure 5–10 Averaging FIR filter input and output responses: (a) with an input sinewave of frequency $f_s/32$; (b) with an input sinewave of frequency $3f_s/32$.

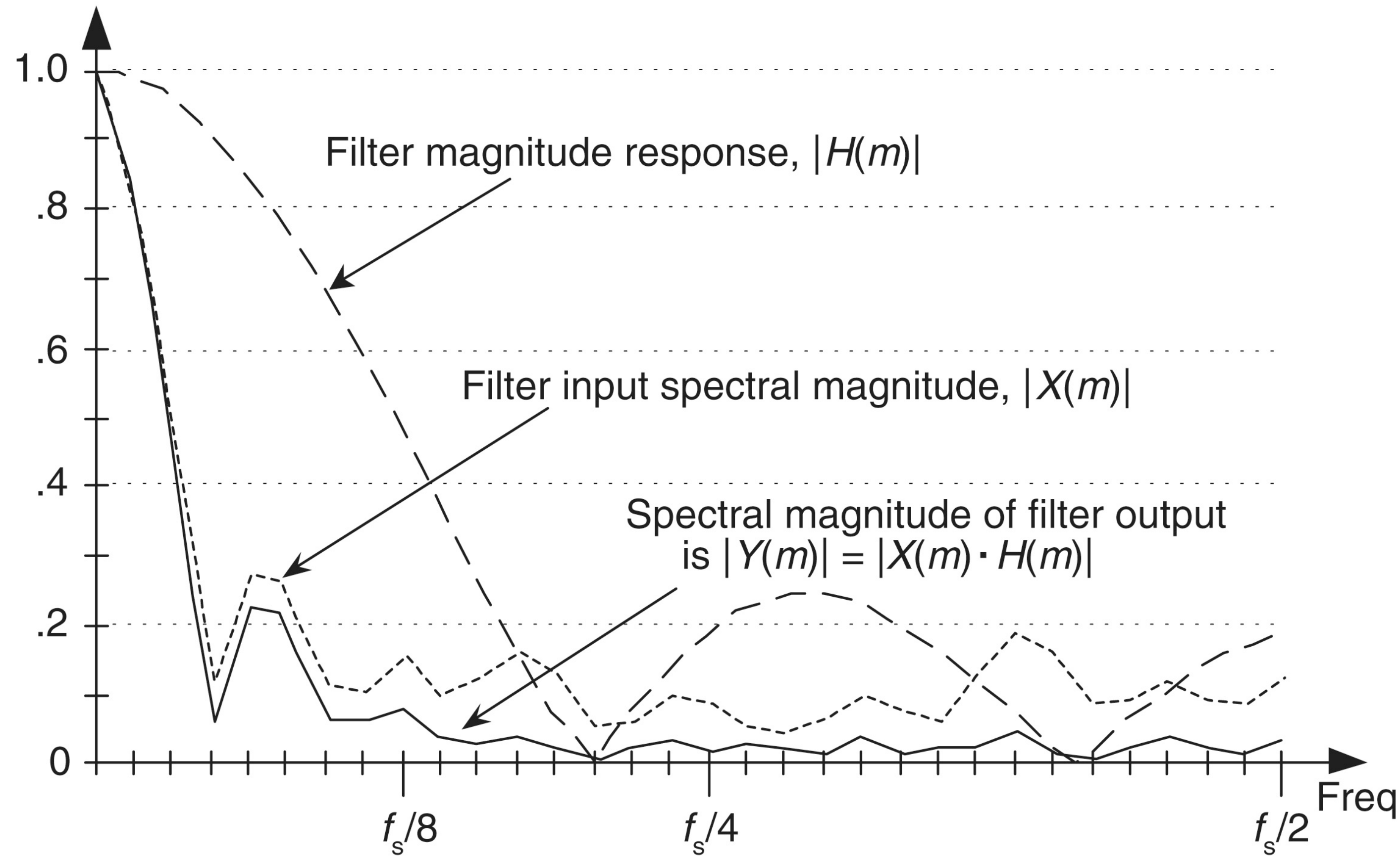

Figure 5–11 Averaging FIR filter input magnitude spectrum, frequency magnitude response, and output magnitude spectrum.

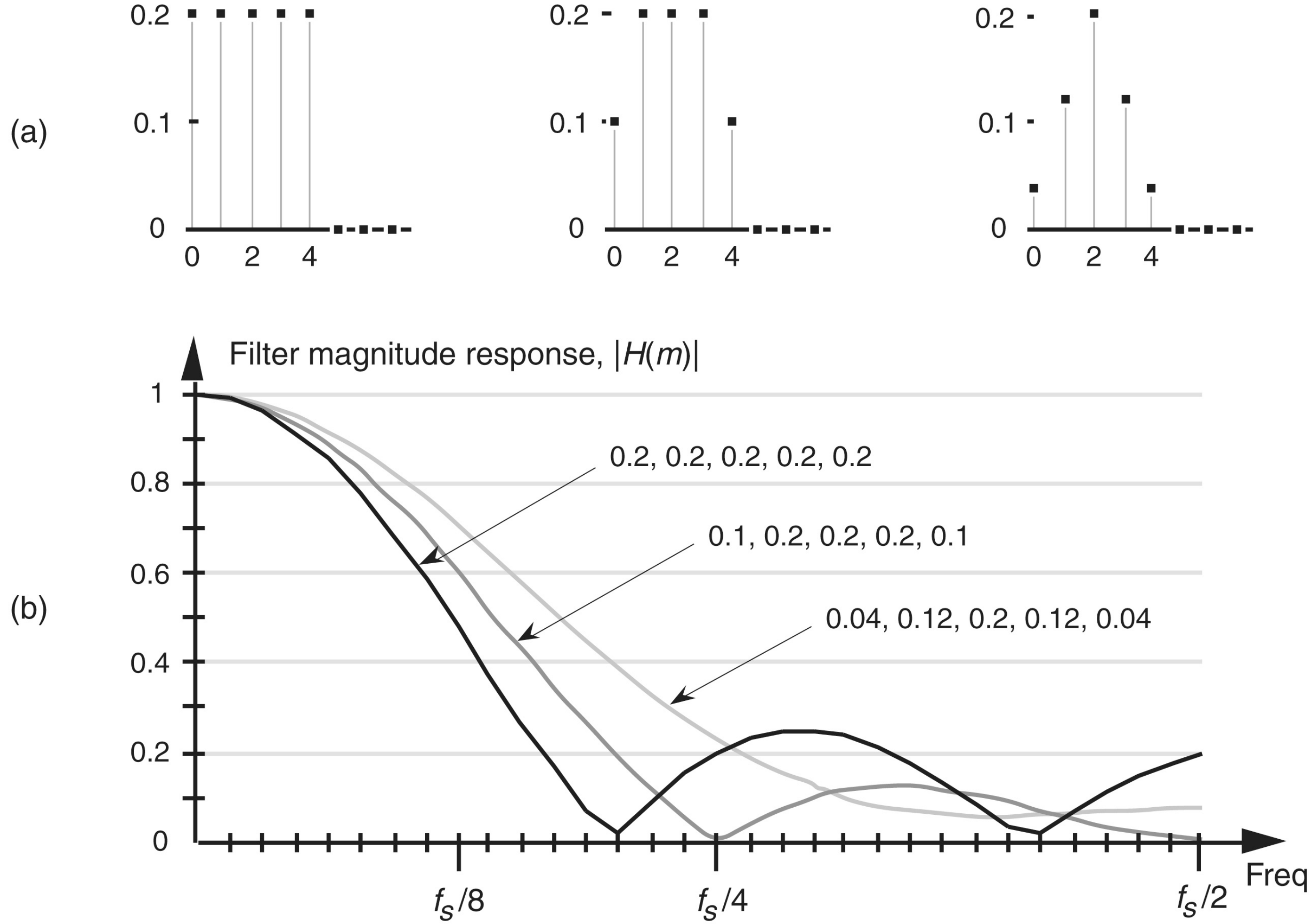

Figure 5–12 Three sets of 5-tap lowpass filter coefficients: (a) sets of coefficients: 0.2, 0.2, 0.2, 0.2, 0.2; 0.1, 0.2, 0.2, 0.2, 0.1; and 0.04, 0.12, 0.2, 0.12, 0.04; (b) frequency magnitude response of three lowpass FIR filters using those sets of coefficients.

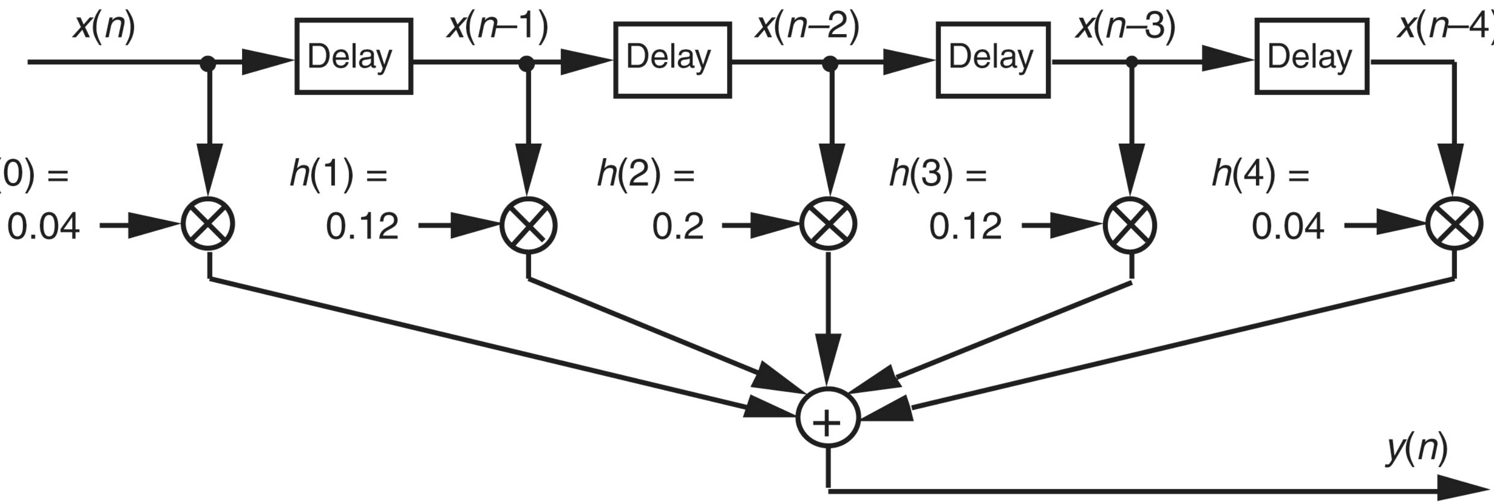

Figure 5–13 Five-tap lowpass FIR filter implementation using the coefficients 0.04, 0.12, 0.2, 0.12, and 0.04.

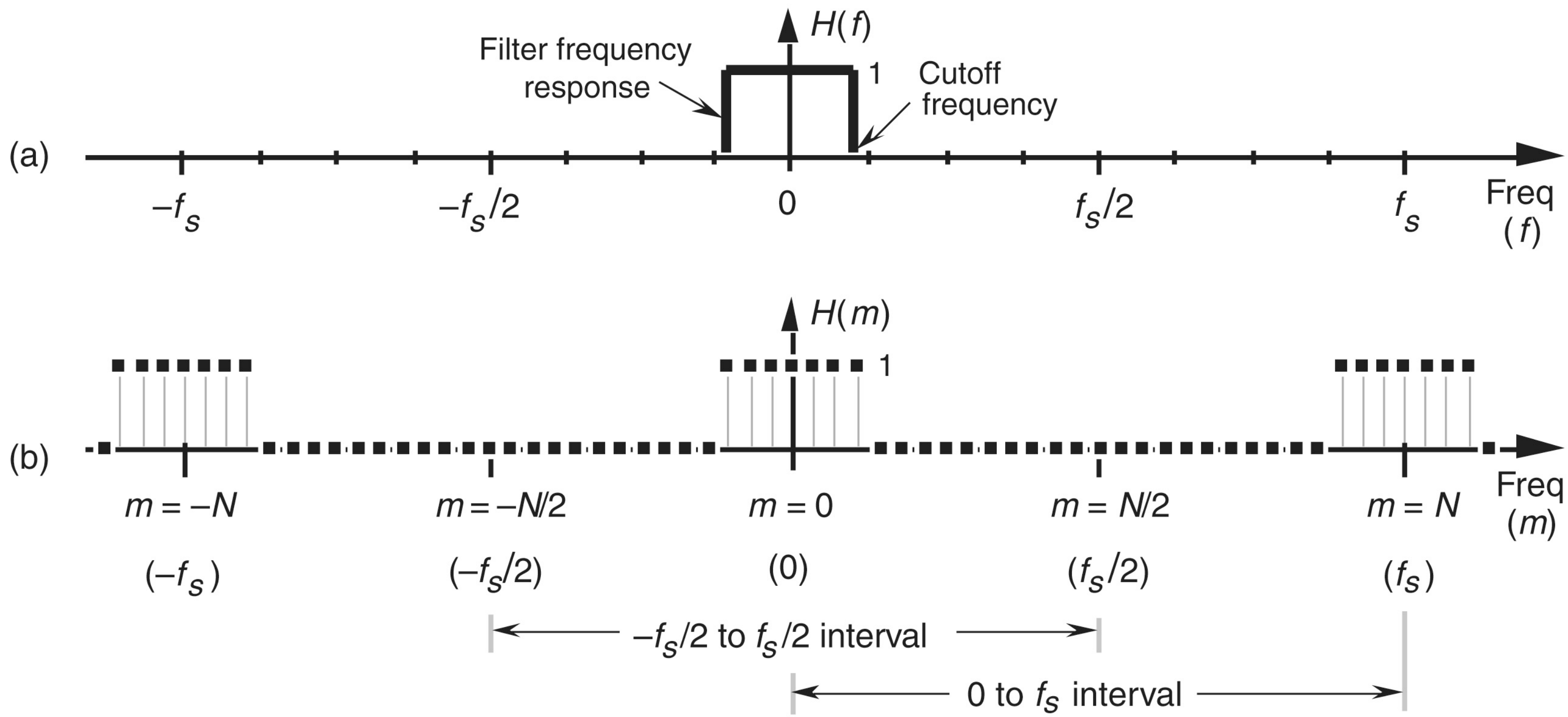

Figure 5–14 Lowpass filter frequency responses: (a) continuous frequency response $H(f)$; (b) periodic, discrete frequency response $H(m)$.

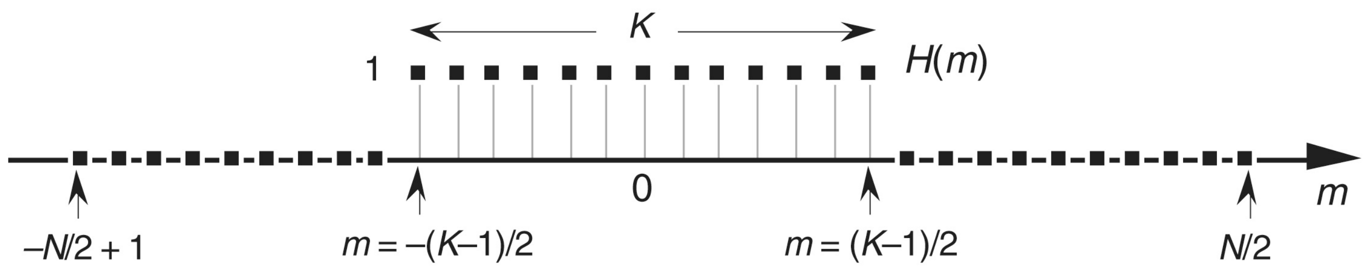

Figure 5–15 Arbitrary, discrete lowpass FIR filter frequency response defined over N frequency-domain samples covering the frequency range of f_s Hz.

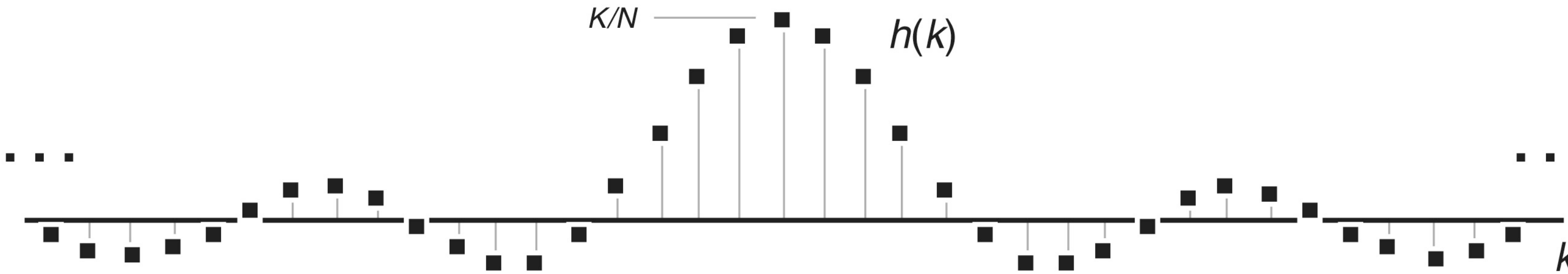

Figure 5–16 Time-domain $h(k)$ coefficients obtained by evaluating Eq. (5–10).

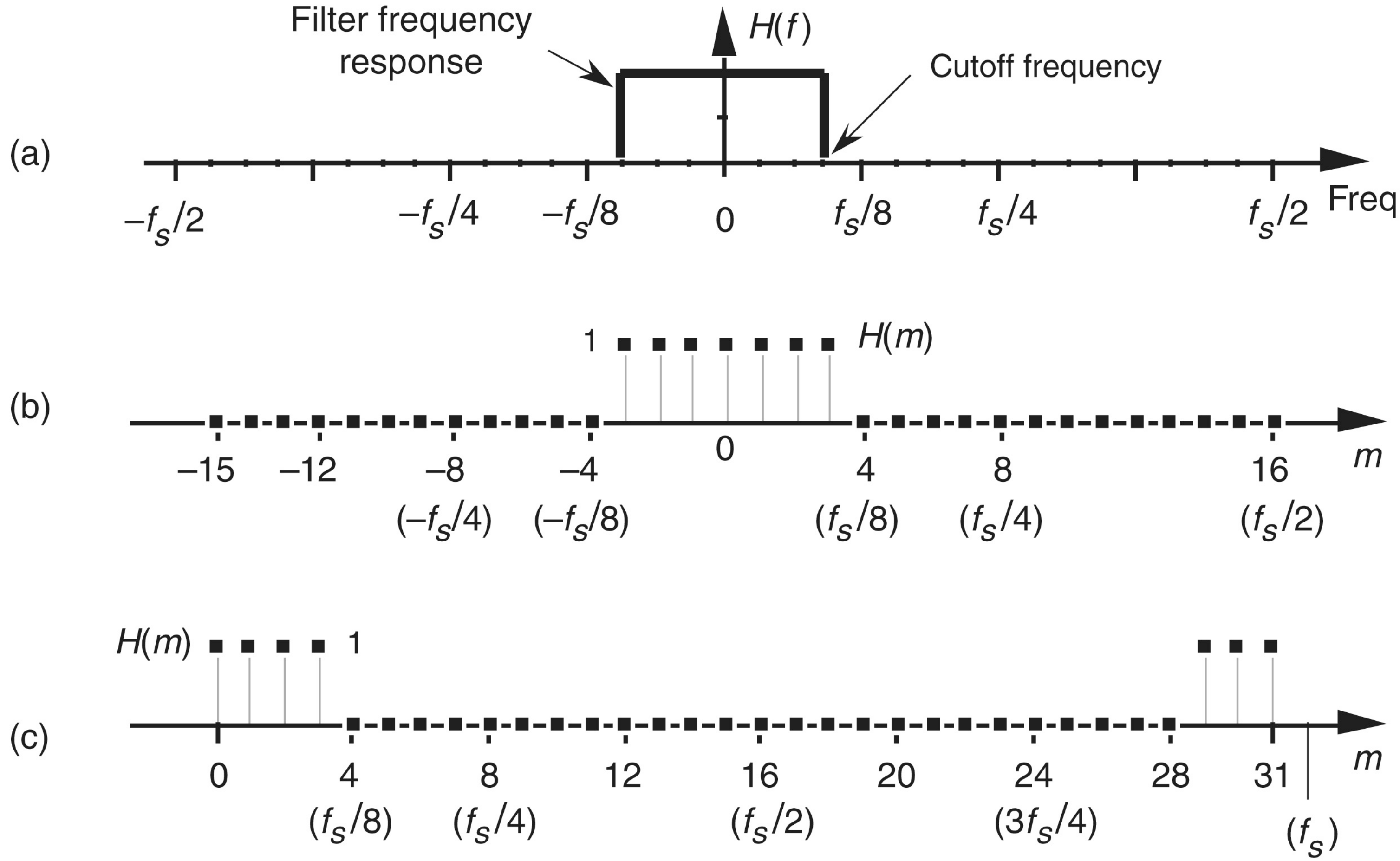

Figure 5–17 An ideal lowpass filter: (a) continuous frequency response $H(f)$; (b) discrete response $H(m)$ over the range $-f_s/2$ to $f_s/2$ Hz; (c) discrete response $H(m)$ over the range 0 to f_s Hz.

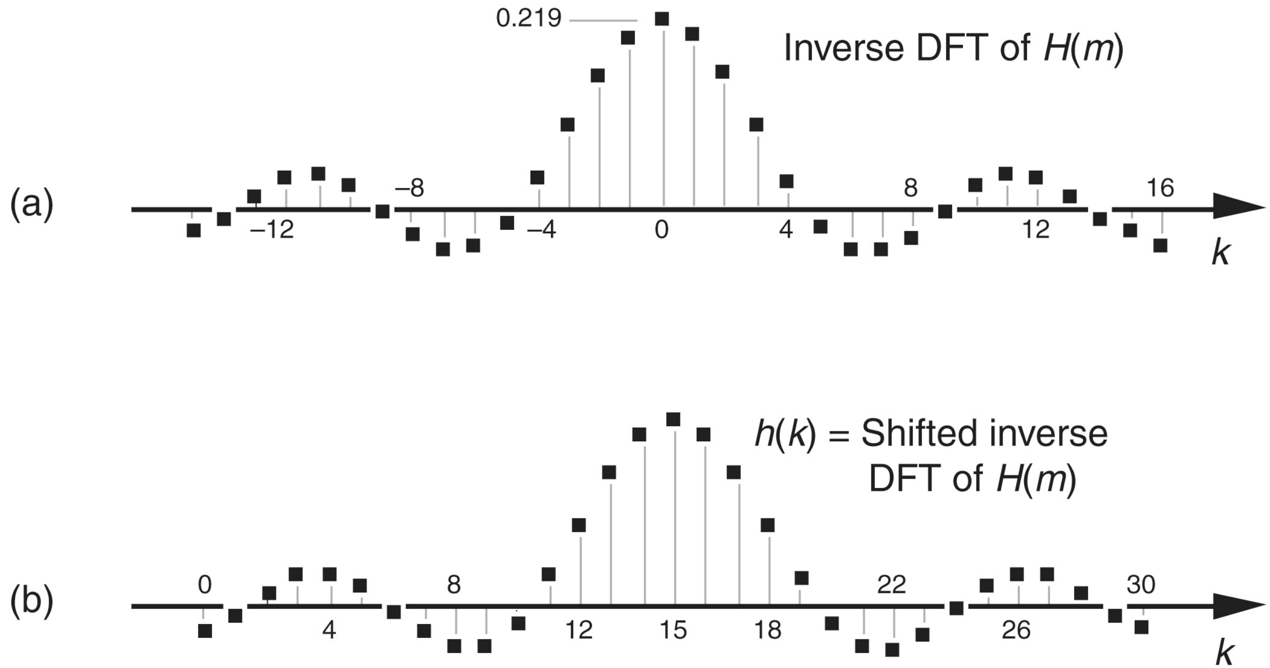

Figure 5–18 Inverse DFT of the discrete response in Figure 5–17(c): (a) normal inverse DFT indexing for *k*; (b) symmetrical coefficients used for a 31-tap lowpass FIR filter.

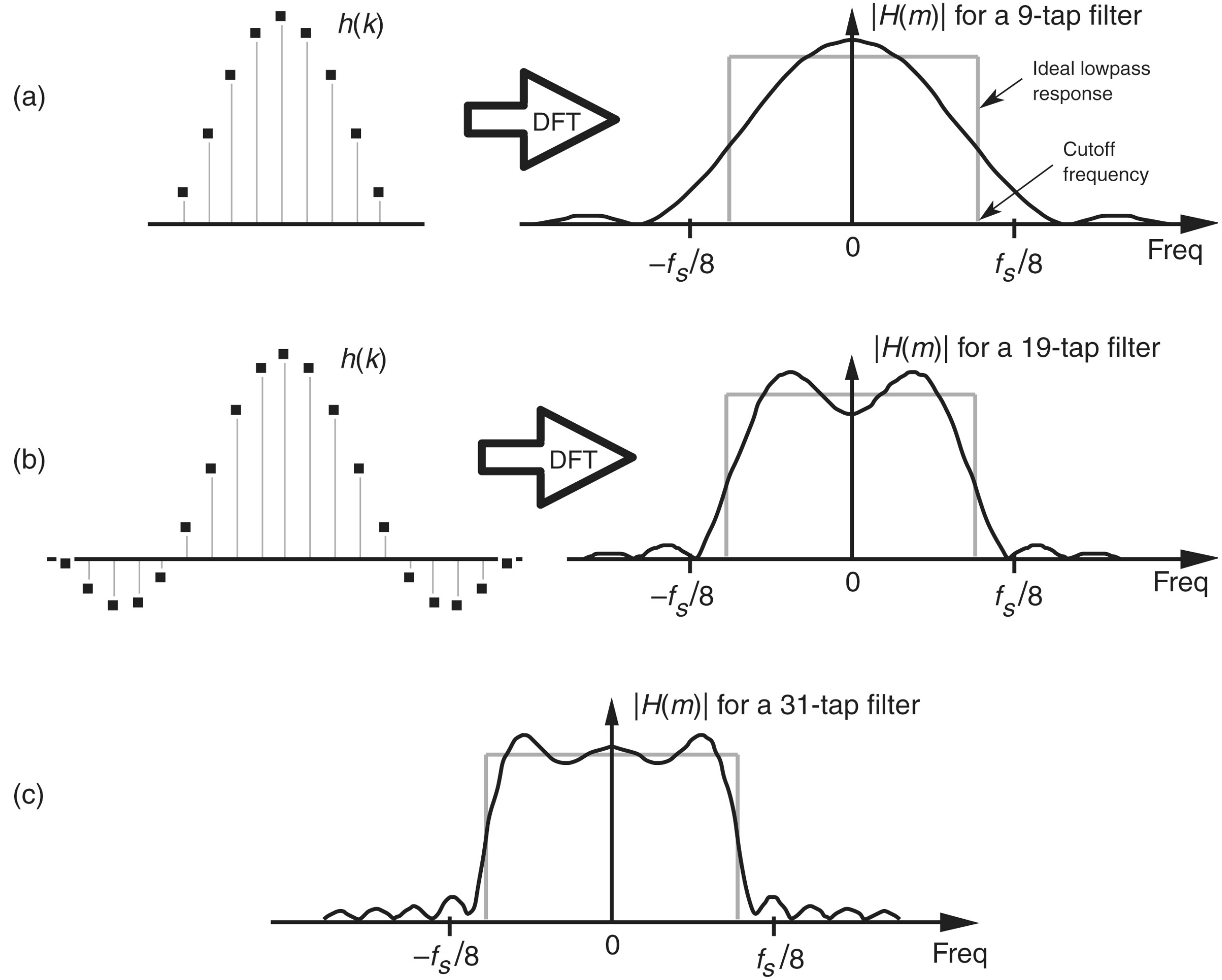

Figure 5–19 Coefficients and frequency responses of three lowpass filters: (a) 9-tap FIR filter; (b) 19-tap FIR filter; (c) frequency response of the full 31-tap FIR filter.

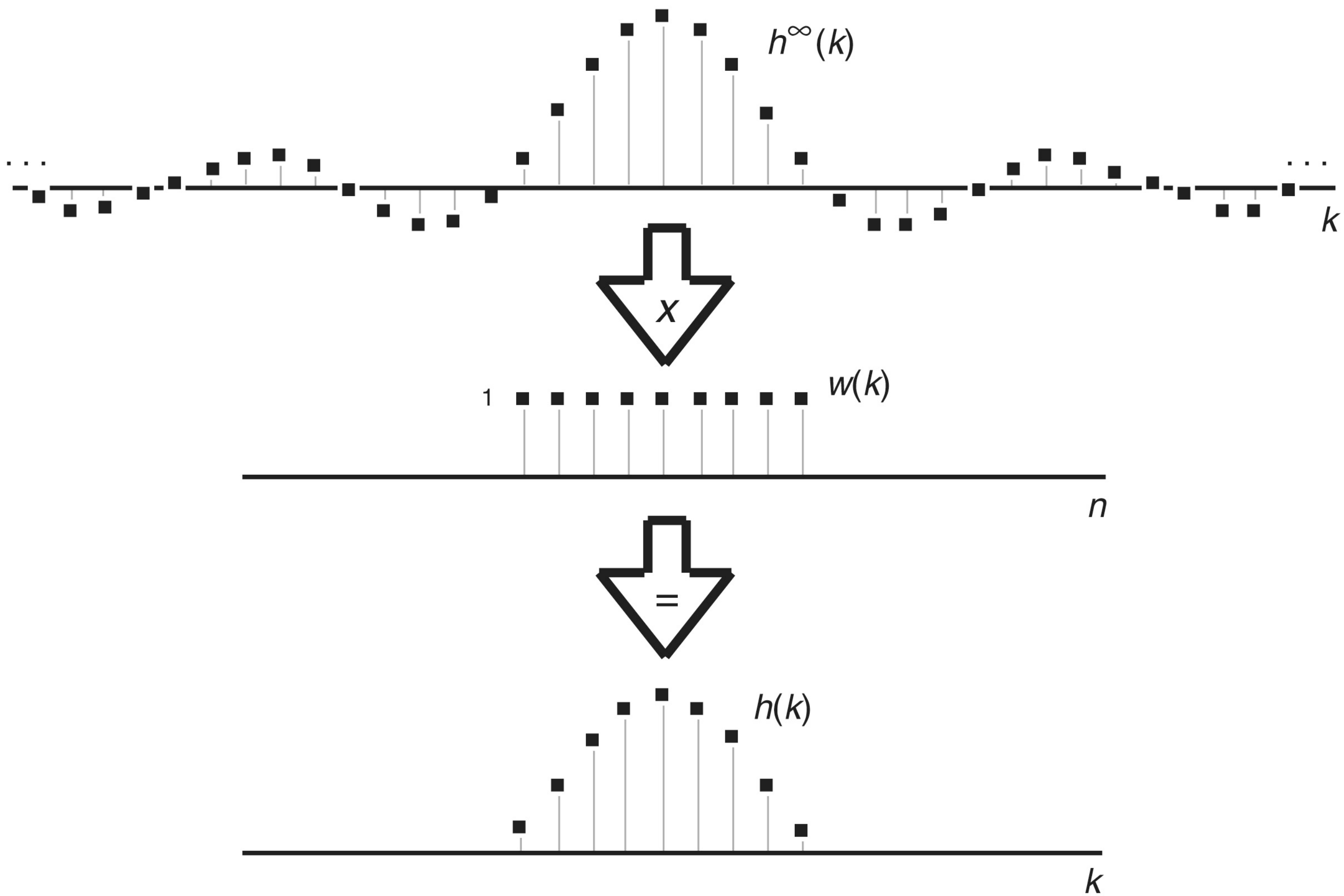

Figure 5–20 Infinite $h^\infty(k)$ sequence windowed by $w(k)$ to define the final filter coefficients $h(k)$.

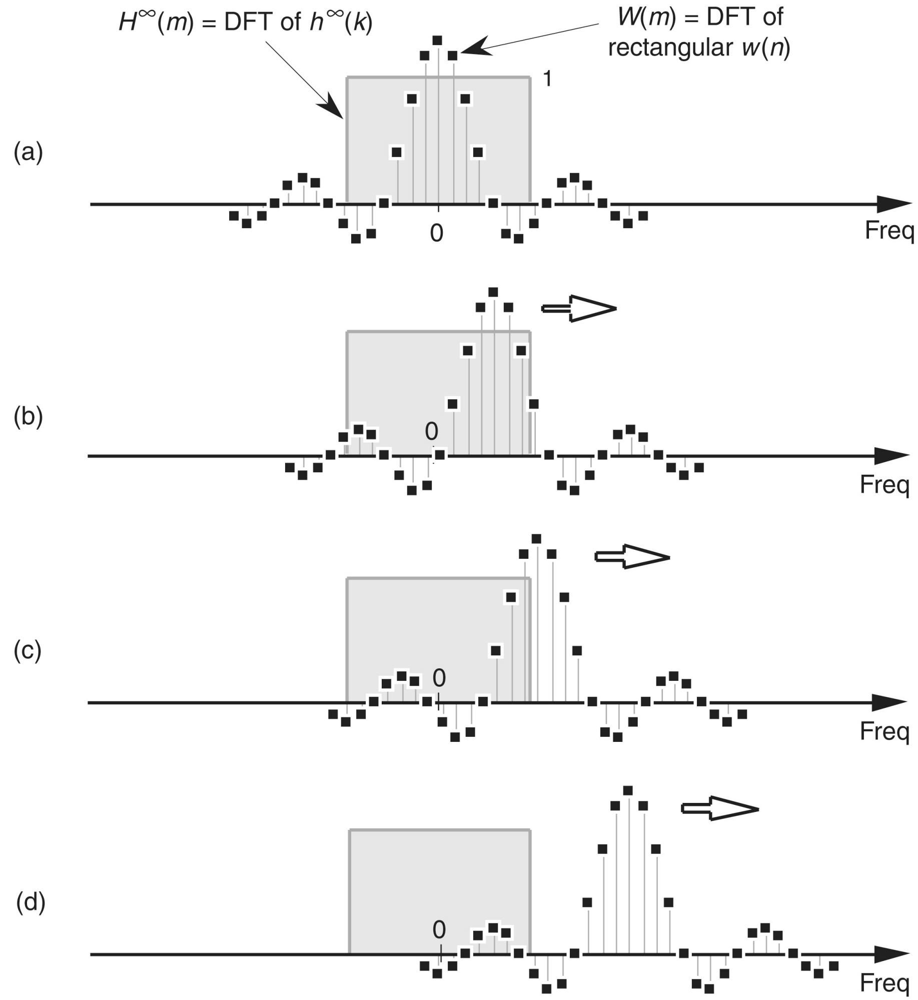

Figure 5–21 Convolution $W(m) * H^\infty(m)$: (a) unshifted $W(m)$ and $H^\infty(m)$; (b) shift of $W(m)$ leading to ripples within $H(m)$'s positive-frequency passband; (c) shift of $W(m)$ causing response roll-off near $H(m)$'s positive cutoff frequency; (d) shift of $W(m)$ causing ripples beyond $H(m)$'s positive cutoff frequency.

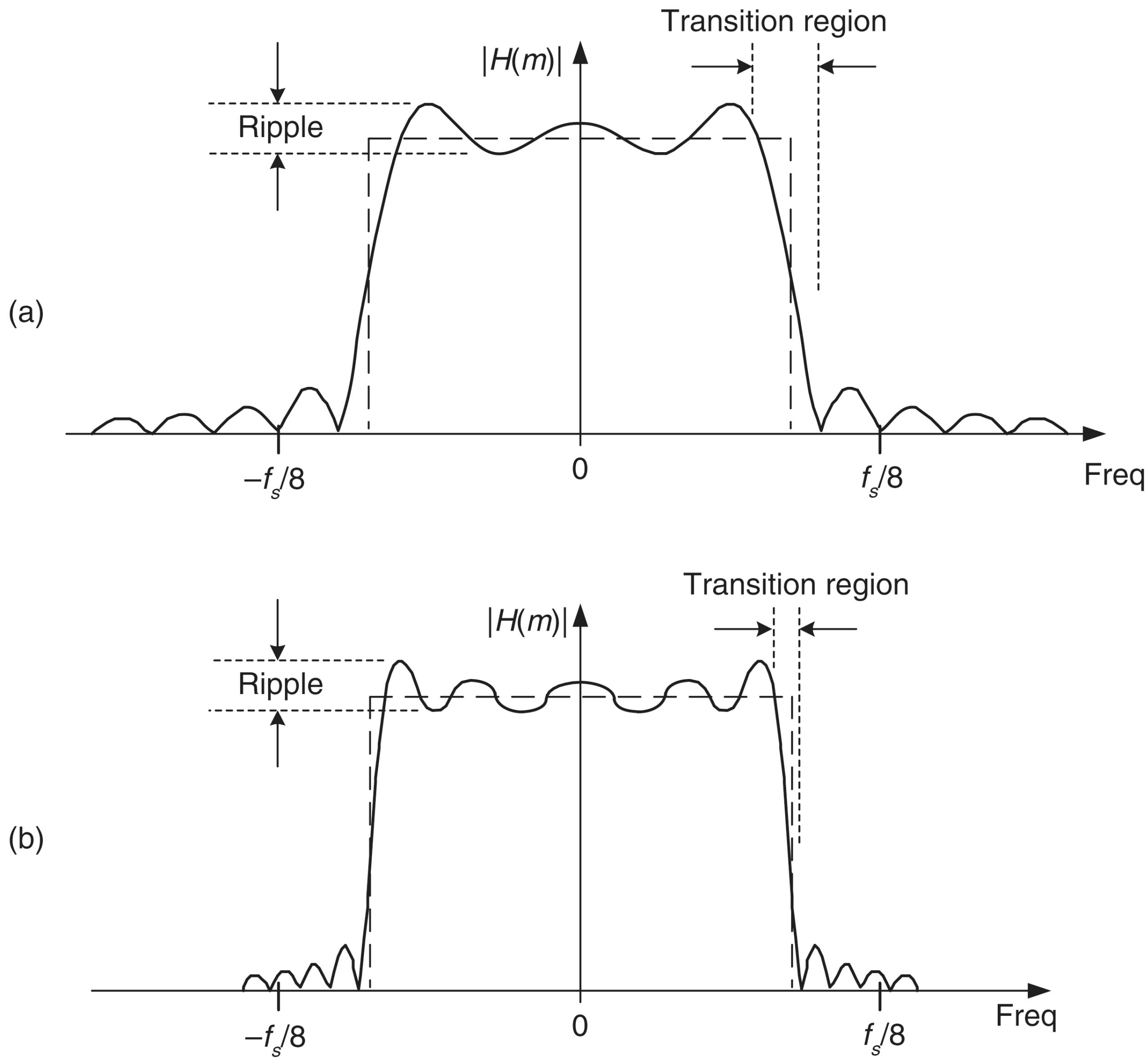

Figure 5–22 Passband ripple and transition regions: (a) for a 31-tap lowpass filter; (b) for a 63-tap lowpass filter.

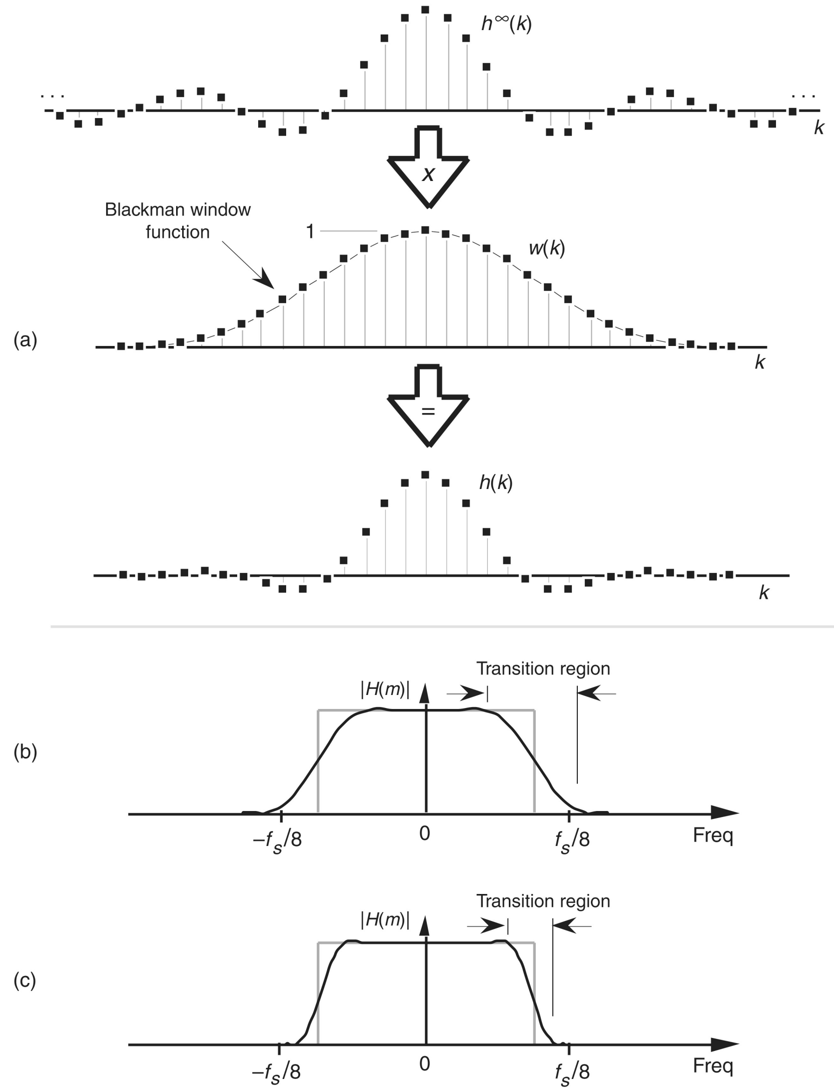

Figure 5–23 Coefficients and frequency response of a 31-tap Blackman-windowed FIR filter: (a) defining the windowed filter coefficients $h(k)$; (b) low-ripple 31-tap frequency response; (c) low-ripple 63-tap frequency response.

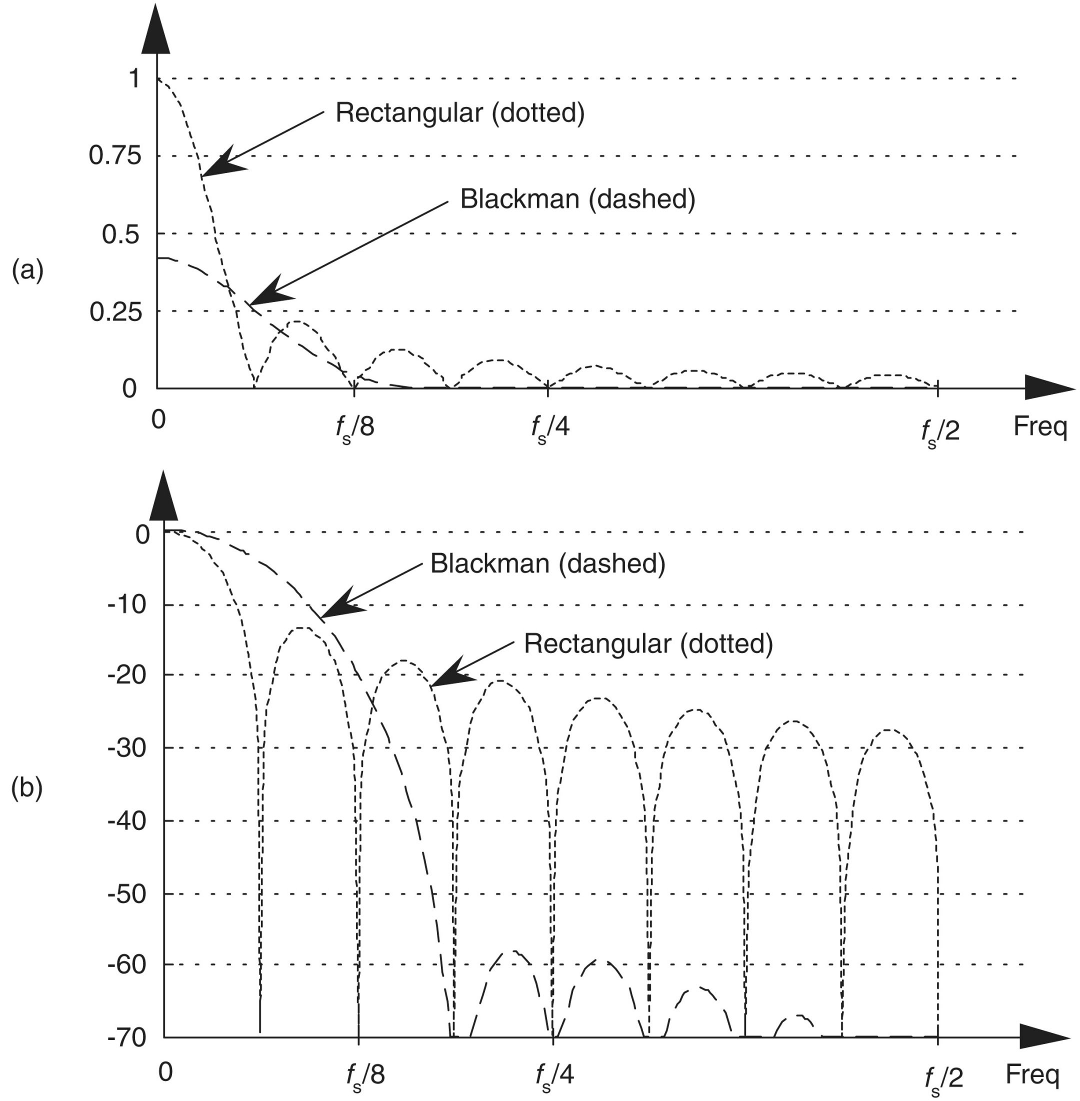

Figure 5–24 Rectangular versus Blackman window frequency magnitude responses: (a) $|W(m)|$ on a linear scale; (b) normalized logarithmic scale of $W_{dB}(m)$.

(a)

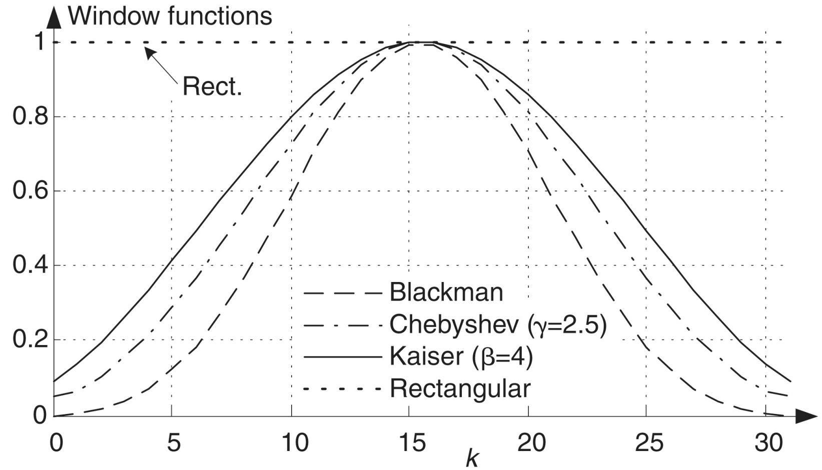

(b)

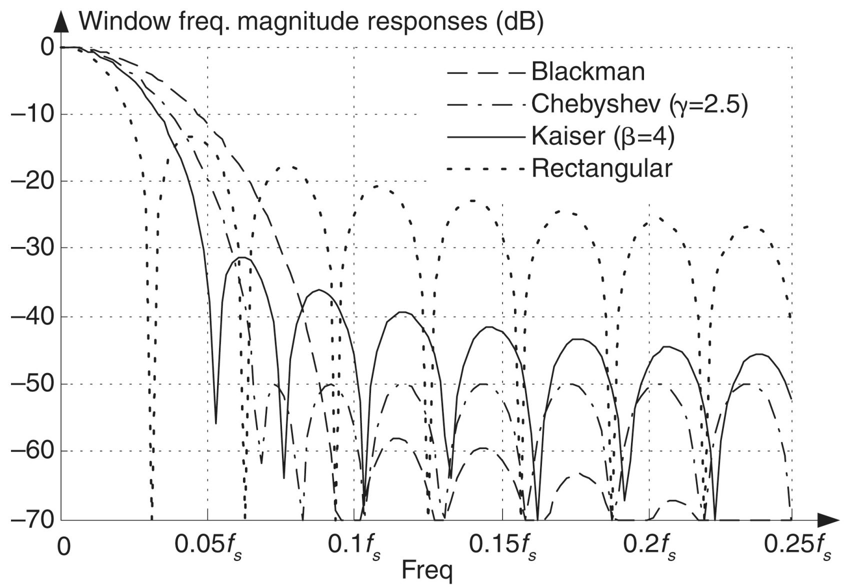

Figure 5–25 Typical window functions used with digital filters: (a) window coefficients in the time domain; (b) frequency-domain magnitude responses in dB.

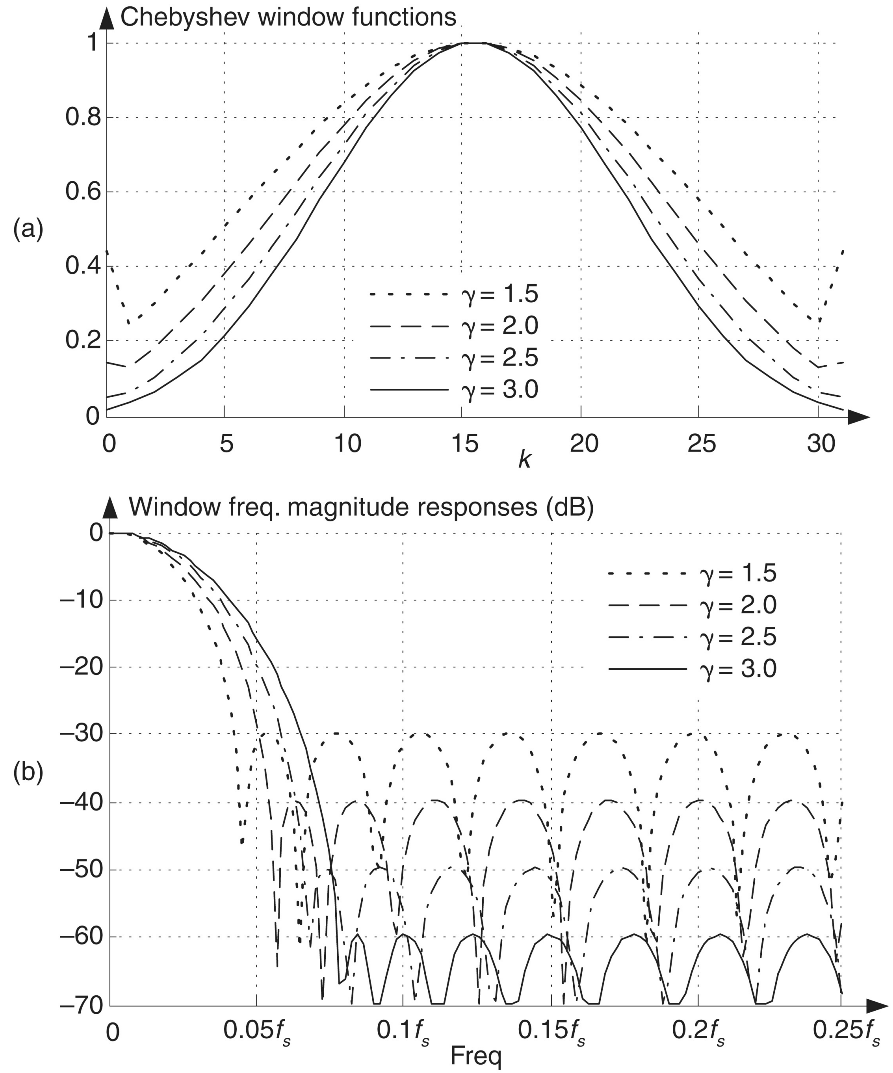

Figure 5–26 Chebyshev window functions for various γ values: (a) window coefficients in the time domain; (b) frequency-domain magnitude responses in dB.

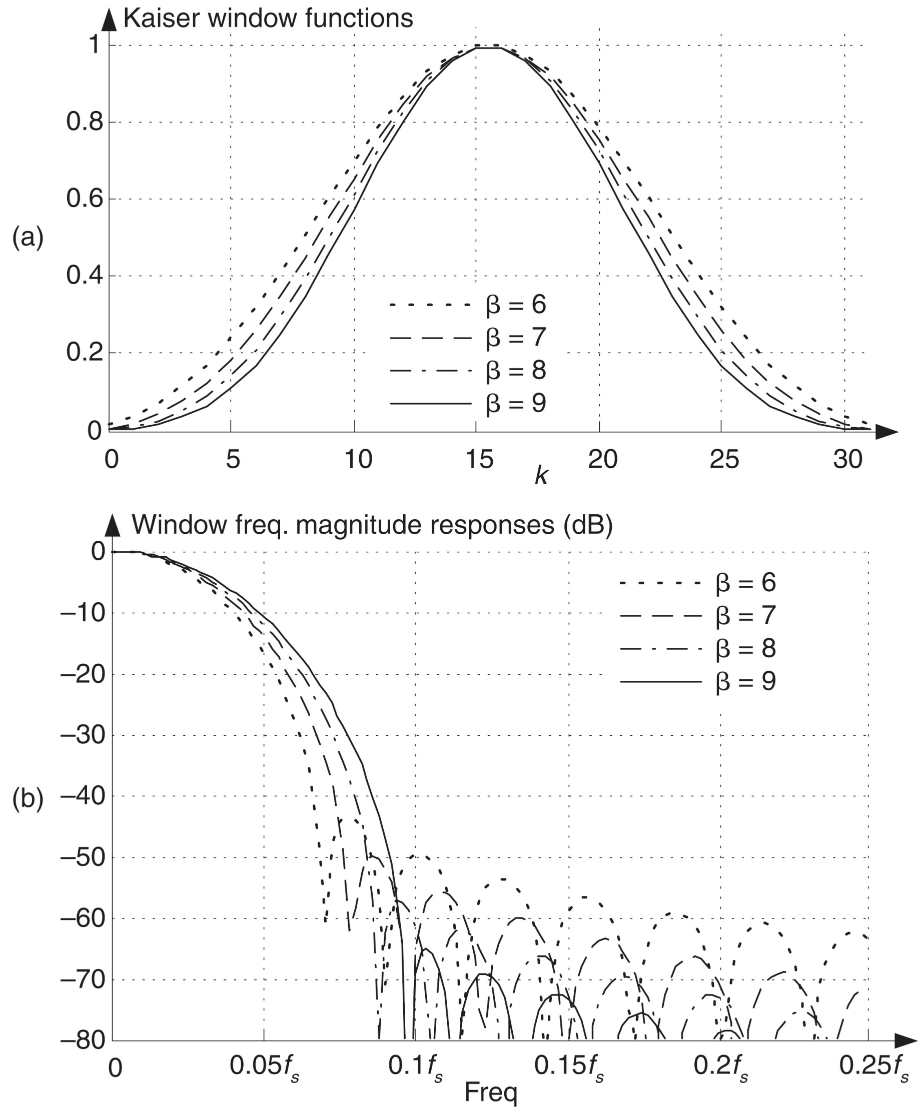

Figure 5–27 Kaiser window functions for various β values: (a) window coefficients in the time domain; (b) frequency-domain magnitude responses in dB.

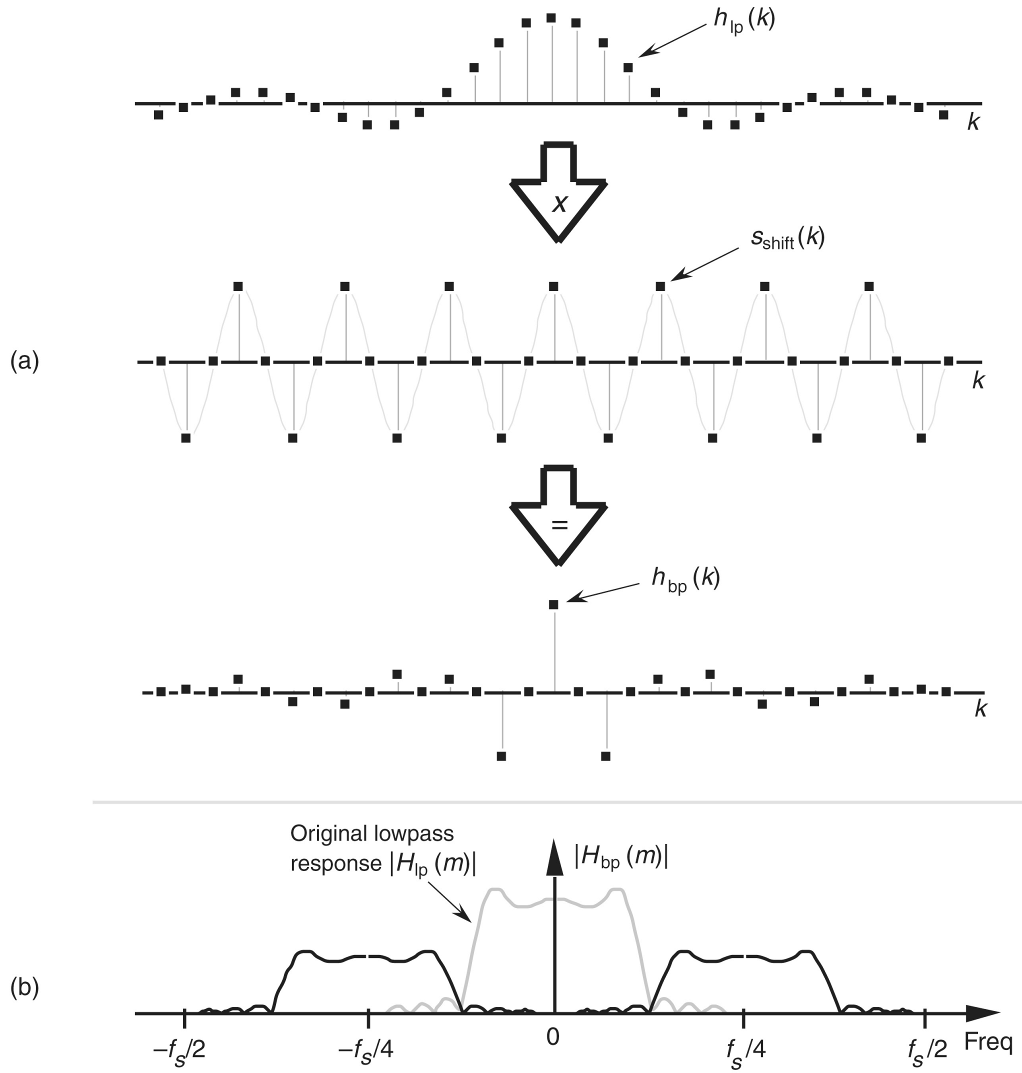

Figure 5–28 Bandpass filter with frequency response centered at $f_s/4$: (a) generating 31-tap filter coefficients $h_{bp}(k)$; (b) frequency magnitude response $|H_{bp}(m)|$.

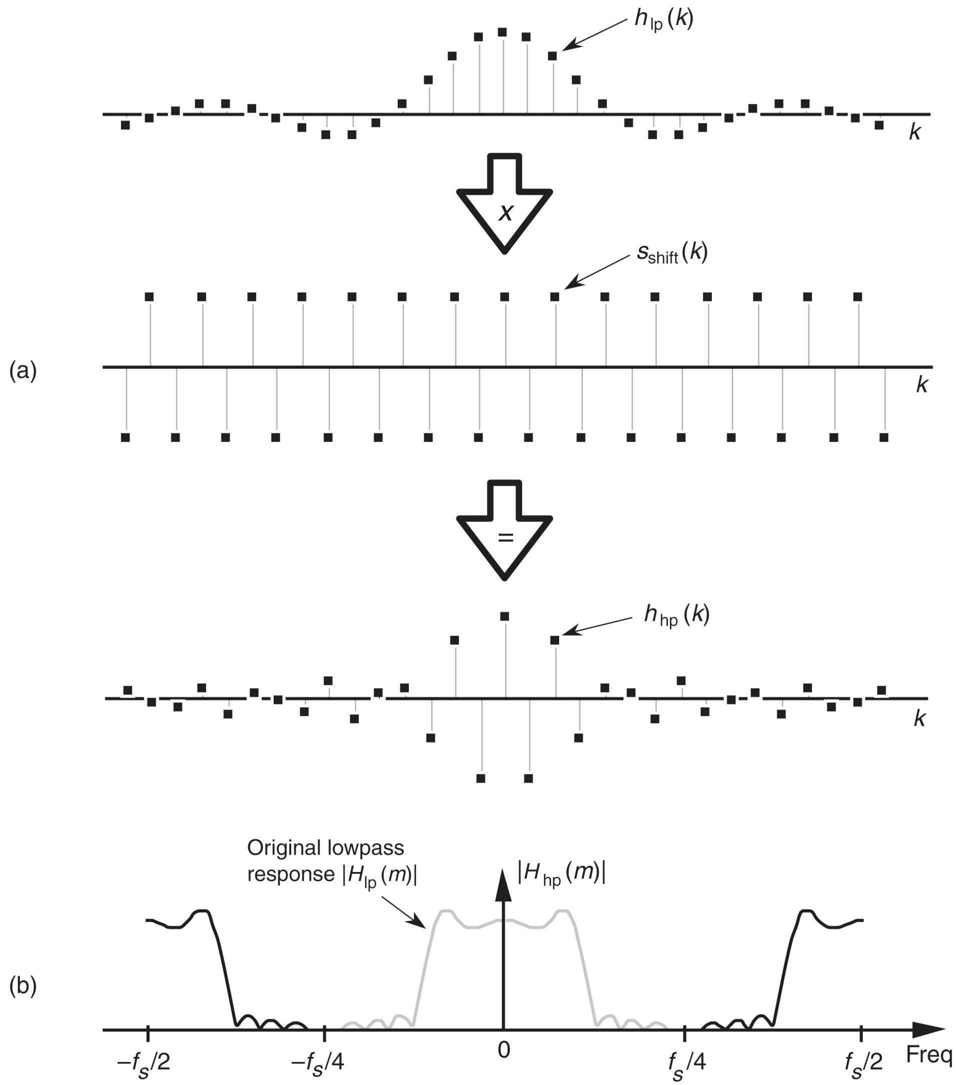

Figure 5–29 Highpass filter with frequency response centered at $f_s/2$: (a) generating 31-tap filter coefficients $h_{hp}(k)$; (b) frequency magnitude response $|H_{hp}(m)|$.

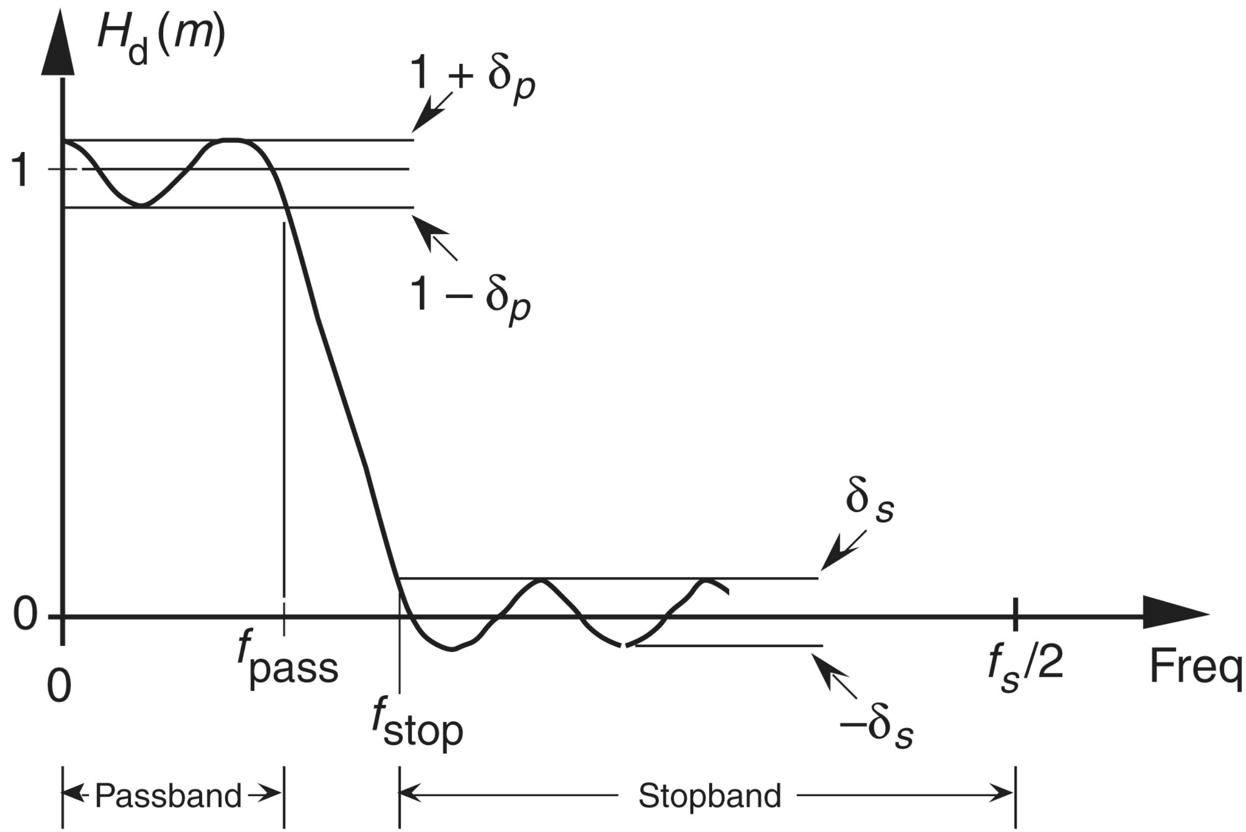

Figure 5–30 Desired frequency response definition of a lowpass FIR filter using the Parks-McClellan Exchange design method.

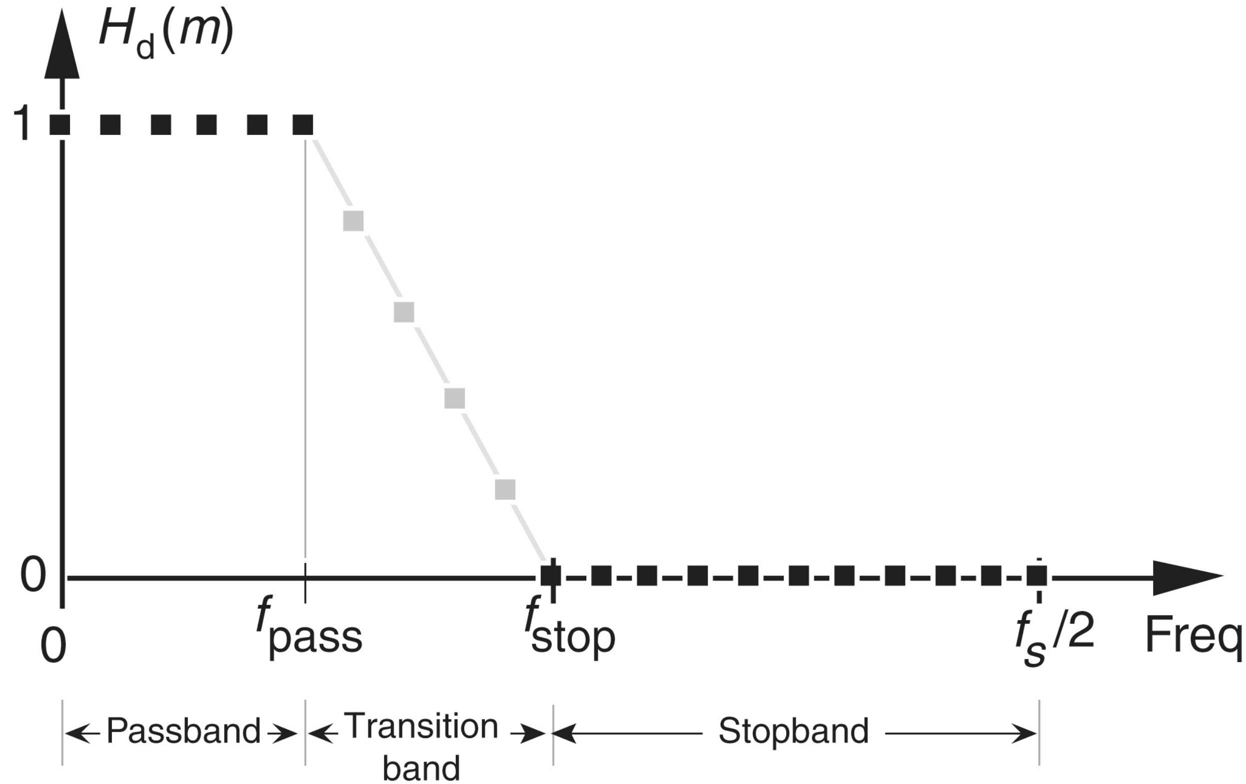

Figure 5–31 Alternate method for defining the desired frequency response of a lowpass FIR filter using the Parks-McClellan Exchange technique.

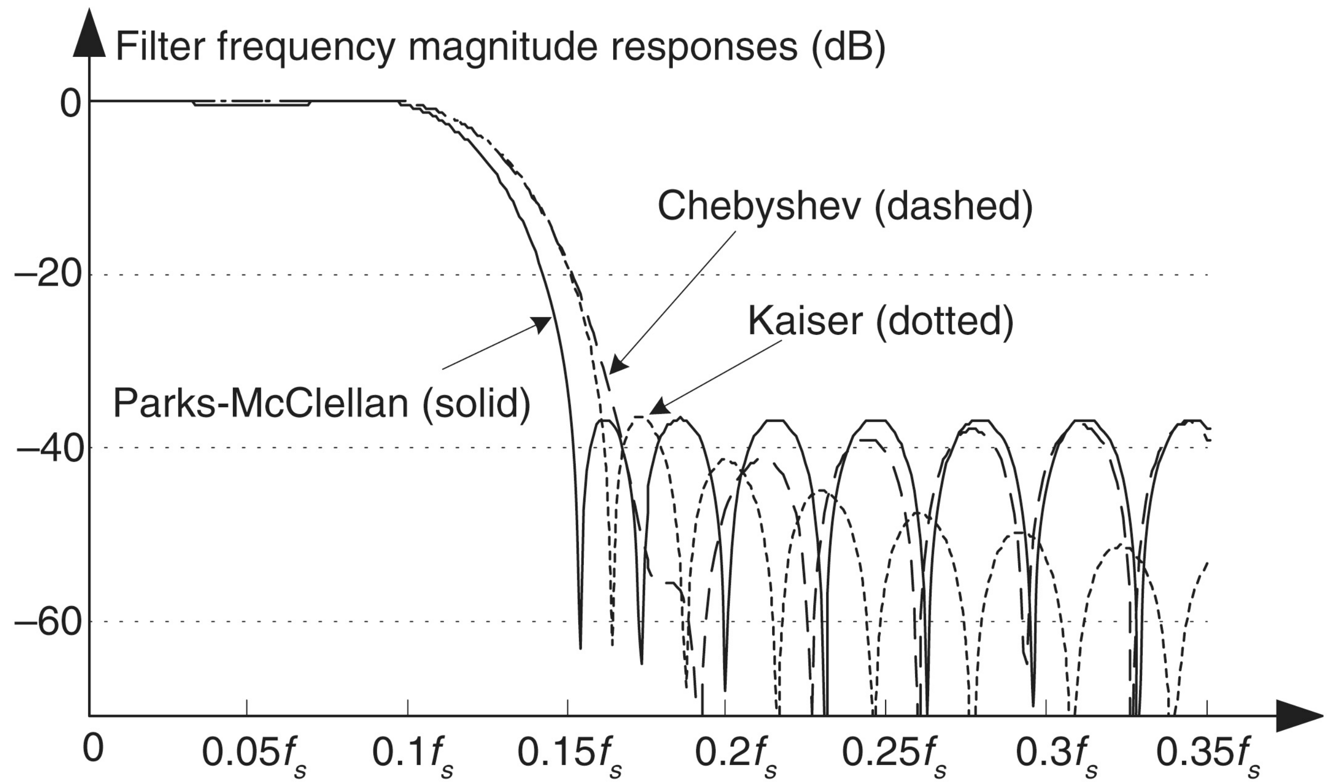

Figure 5–32 Frequency response comparison of three 31-tap FIR filters: Parks-McClellan, Chebyshev windowed, and Kaiser windowed.

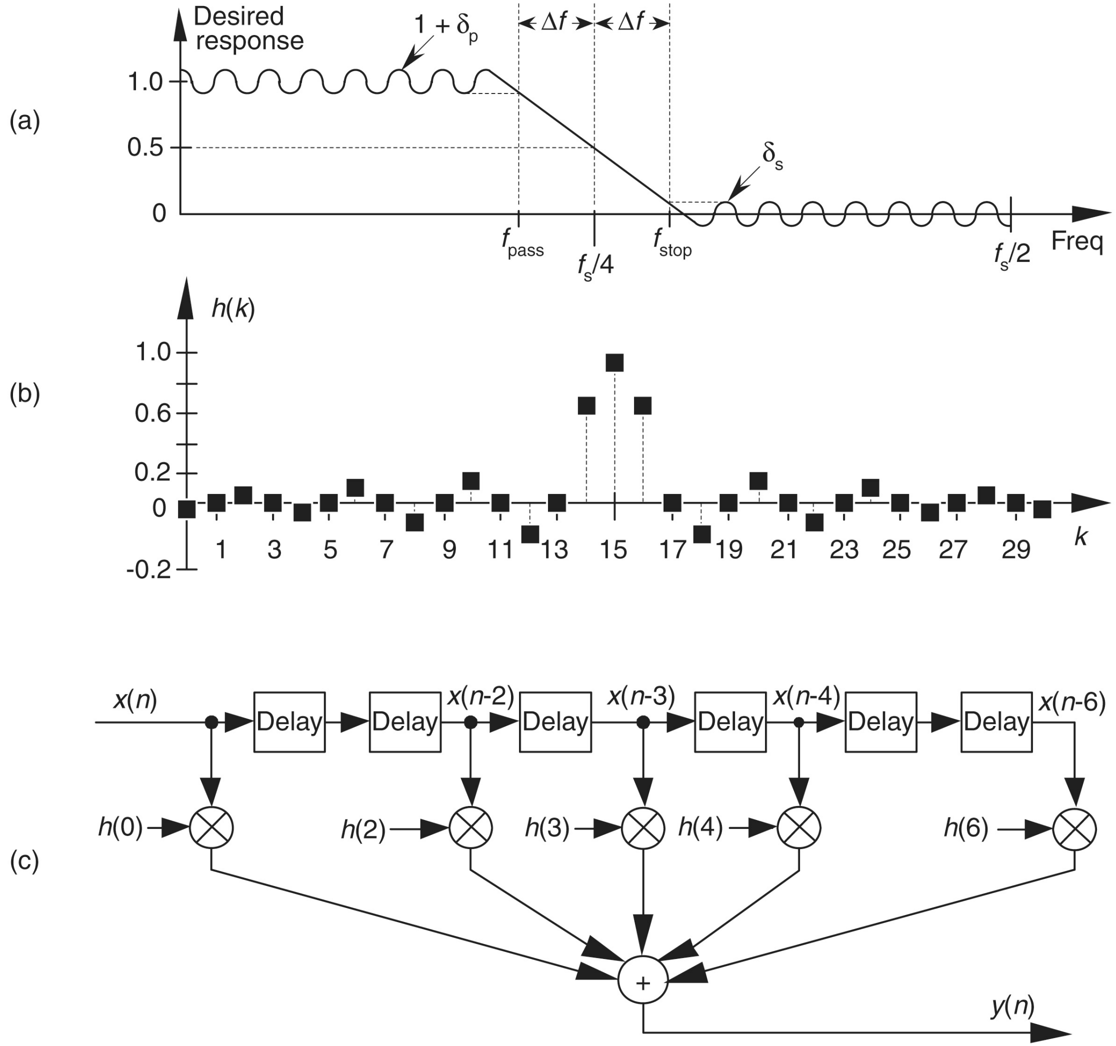

Figure 5-33 Half-band FIR filter: (a) frequency magnitude response (transition region centered at $f_s/4$); (b) 31-tap filter coefficients; (c) 7-tap half-band filter structure.

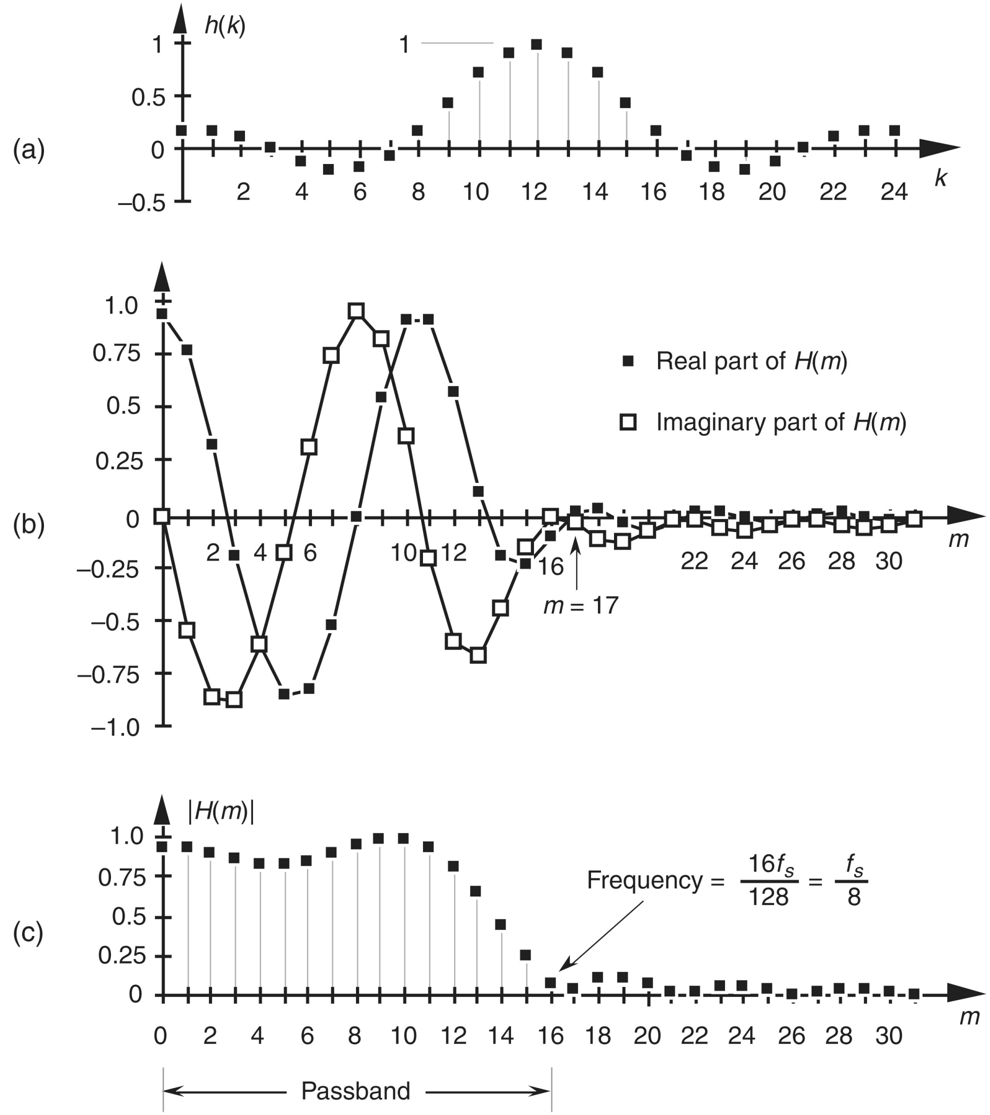

Figure 5–34 FIR filter frequency response $H(m)$: (a) $h(k)$ filter coefficients; (b) real and imaginary parts of $H(m)$; (c) magnitude of $H(m)$.

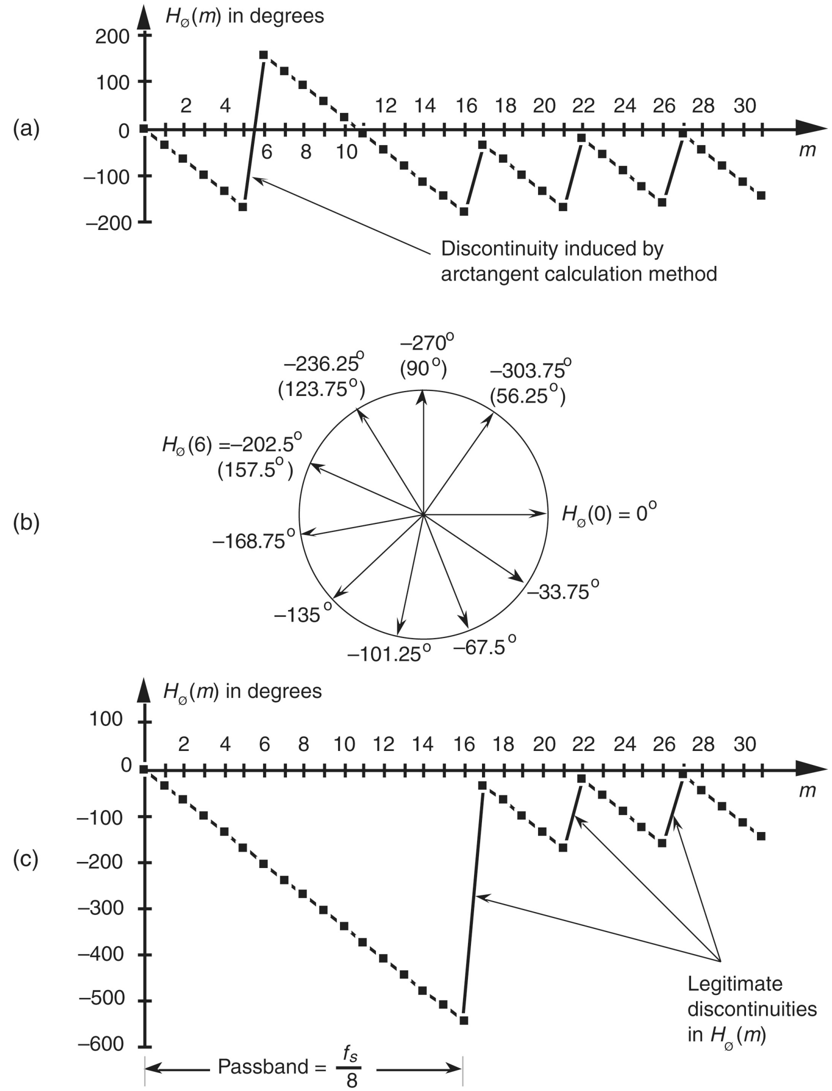

Figure 5–35 FIR filter phase response $H_ø(m)$ in degrees: (a) calculated $H_ø(m)$; (b) polar plot of $H_ø(m)$'s first ten phase angles in degrees; (c) actual $H_ø(m)$.

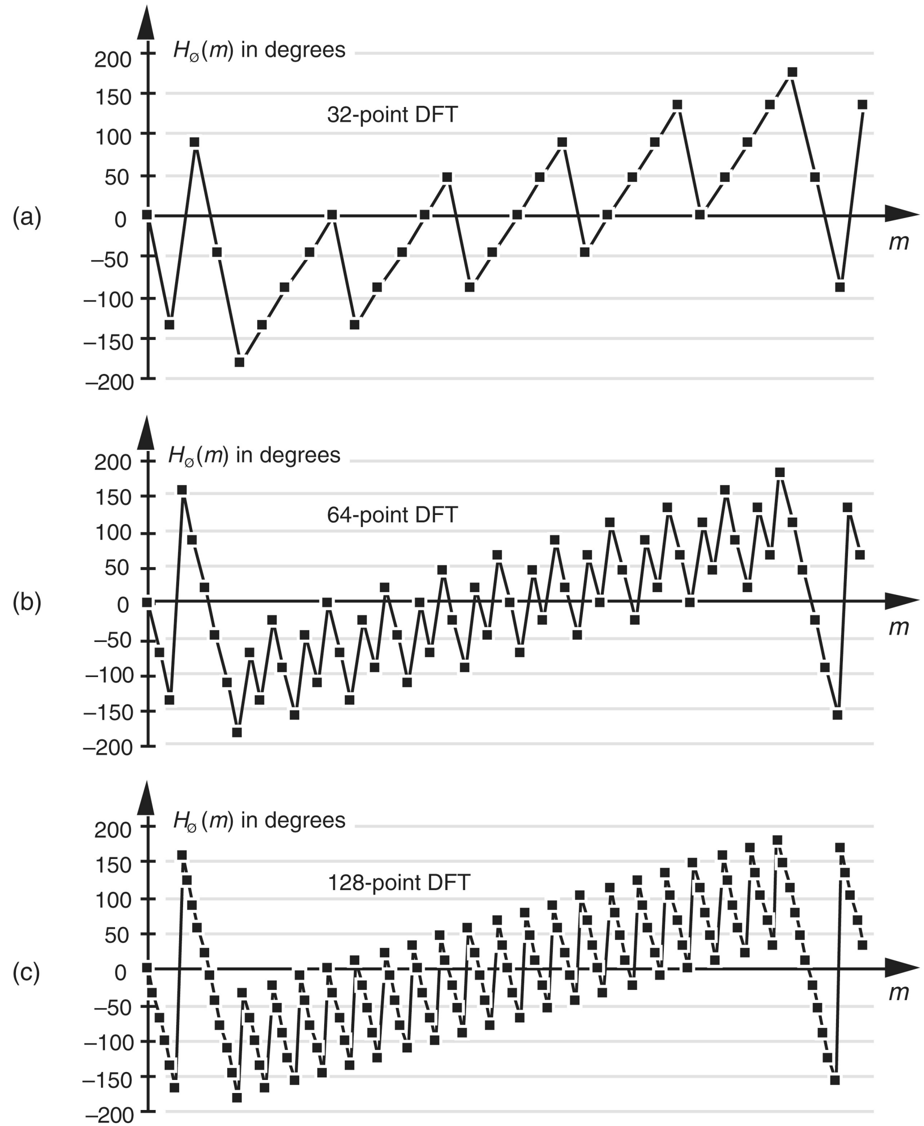

Figure 5–36 FIR filter phase response $H_ø(m)$ in degrees: (a) calculated using a 32-point DFT; (b) using a 64-point DFT; (c) using a 128-point DFT.

$$Y_j = \sum_{k=0}^{N-1} P_k \cdot Q_{j-k}, \quad \text{or}$$

$$\begin{bmatrix} Y_0 \\ Y_1 \\ Y_2 \\ . \\ . \\ . \\ Y_{N-1} \end{bmatrix} = \begin{bmatrix} Q_0 & Q_{N-1} & Q_{N-2} & \cdots & Q_1 \\ Q_1 & Q_0 & Q_{N-1} & \cdots & Q_2 \\ Q_2 & Q_1 & Q_0 & \cdots & Q_3 \\ . & . & . & . & . \\ . & . & . & . & . \\ . & . & . & . & . \\ Q_{N-1} & Q_{N-2} & Q_{N-3} & \cdots & Q_0 \end{bmatrix} \cdot \begin{bmatrix} P_0 \\ P_1 \\ P_2 \\ . \\ . \\ . \\ P_{N-1} \end{bmatrix}$$

Theorem: if

$$P_j \leftarrow \text{DFT} \rightarrow A_n \;,$$

$$Q_j \leftarrow \text{DFT} \rightarrow B_n \;, \text{ and}$$

$$Y_j \leftarrow \text{DFT} \rightarrow C_n \;,$$

then

$$C_n = N \cdot A_n \cdot B_n .$$

Figure 5–37 One very efficient, but perplexing, way of defining convolution.

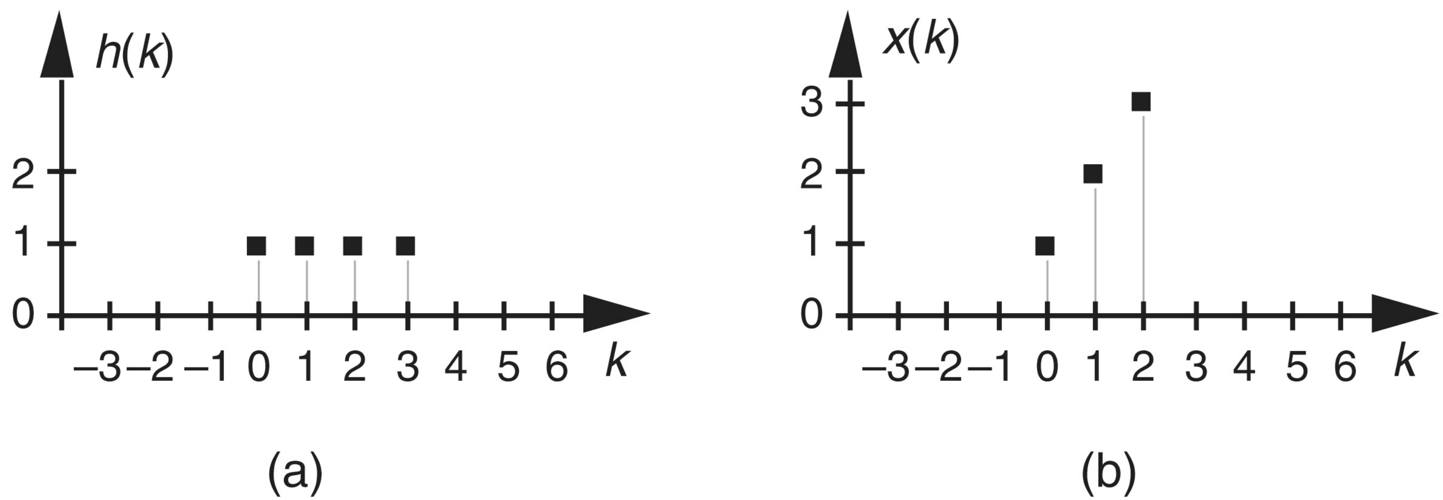

Figure 5–38 Convolution example input sequences: (a) first sequence $h(k)$ of length $P = 4$; (b) second sequence $x(k)$ of length $Q = 3$.

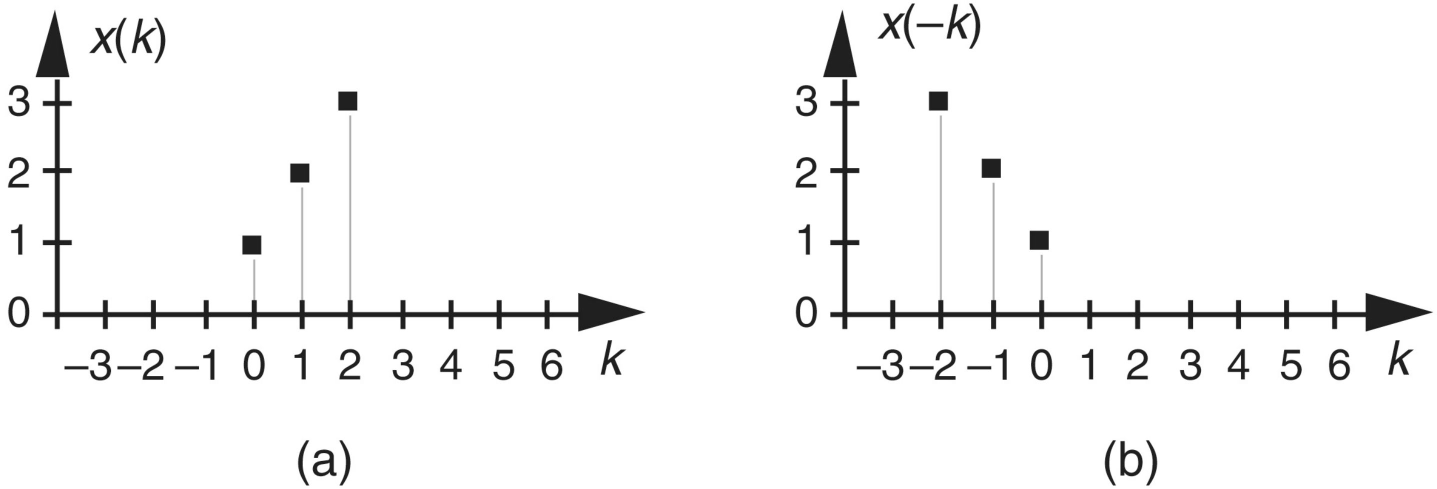

Figure 5–39 Convolution example input sequence: (a) second sequence $x(k)$ of length 3; (b) reflection of the second sequence about the $k = 0$ index.

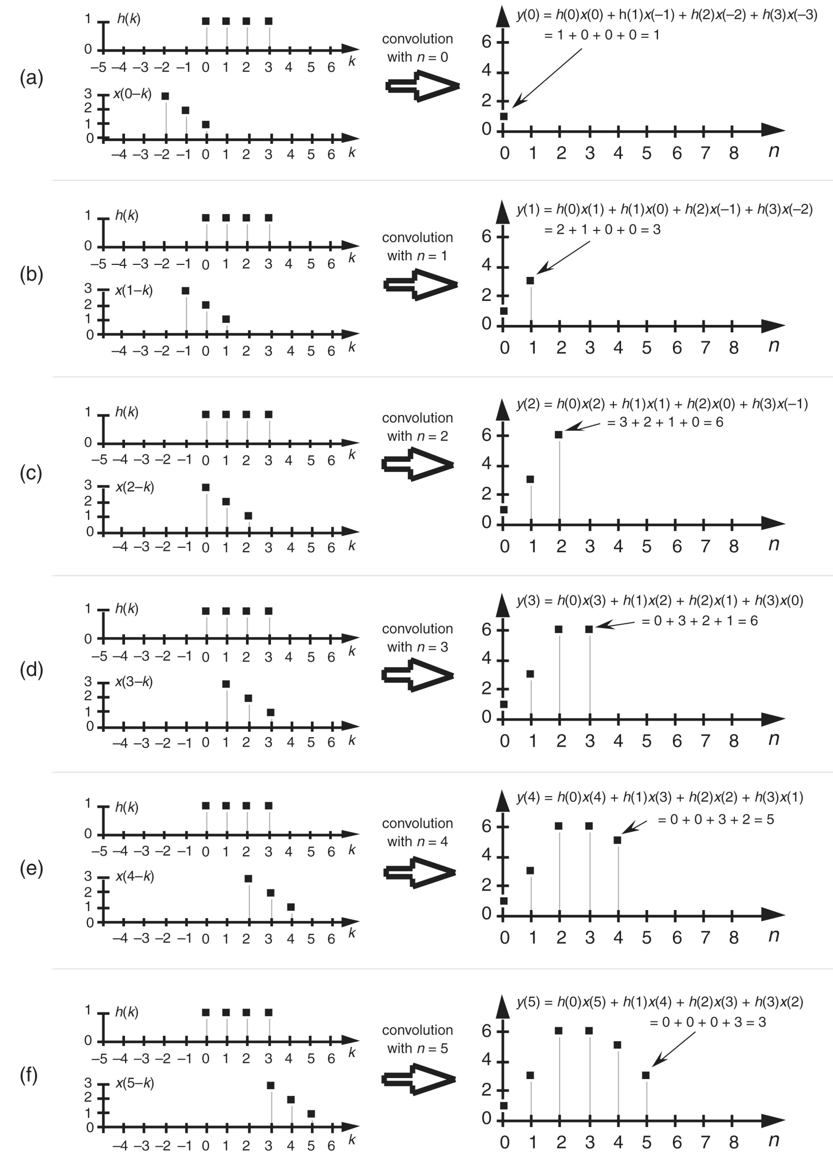

Figure 5–40 Graphical depiction of the convolution of $h(k)$ and $x(k)$ in Figure 5–38.

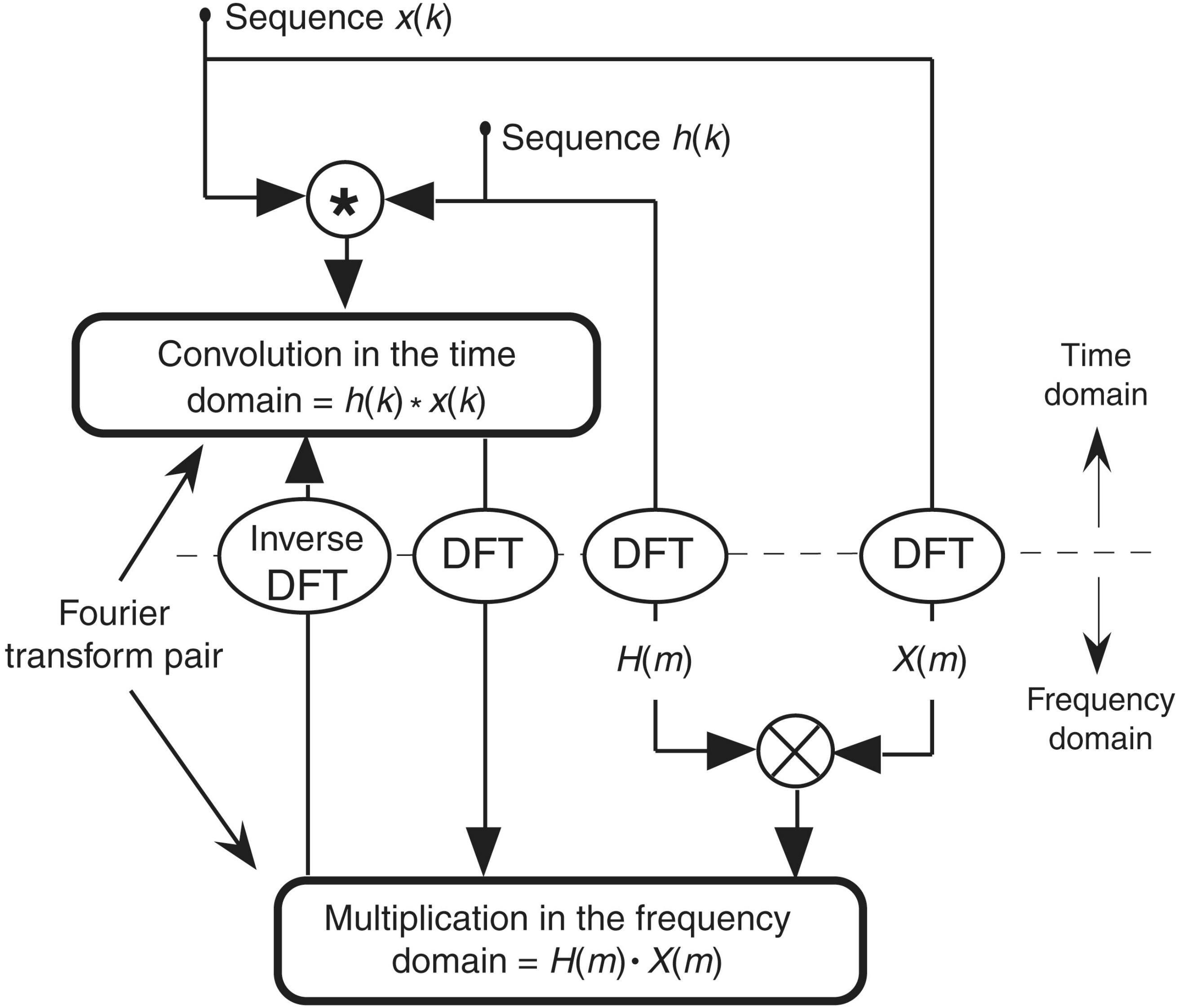

Figure 5–41 Relationships of the convolution theorem.

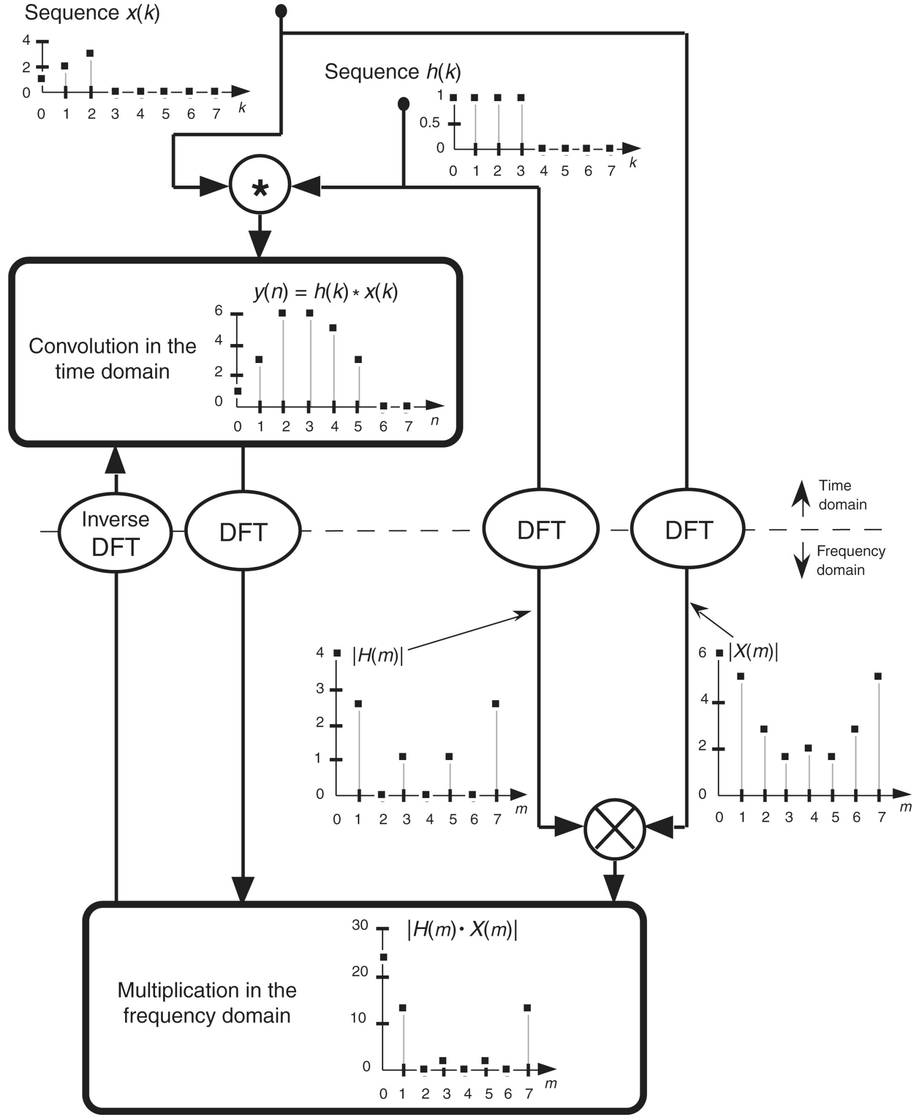

Figure 5–42 Convolution relationships of $h(k)$, $x(k)$, $H(m)$, and $X(m)$ from Figure 5–38.

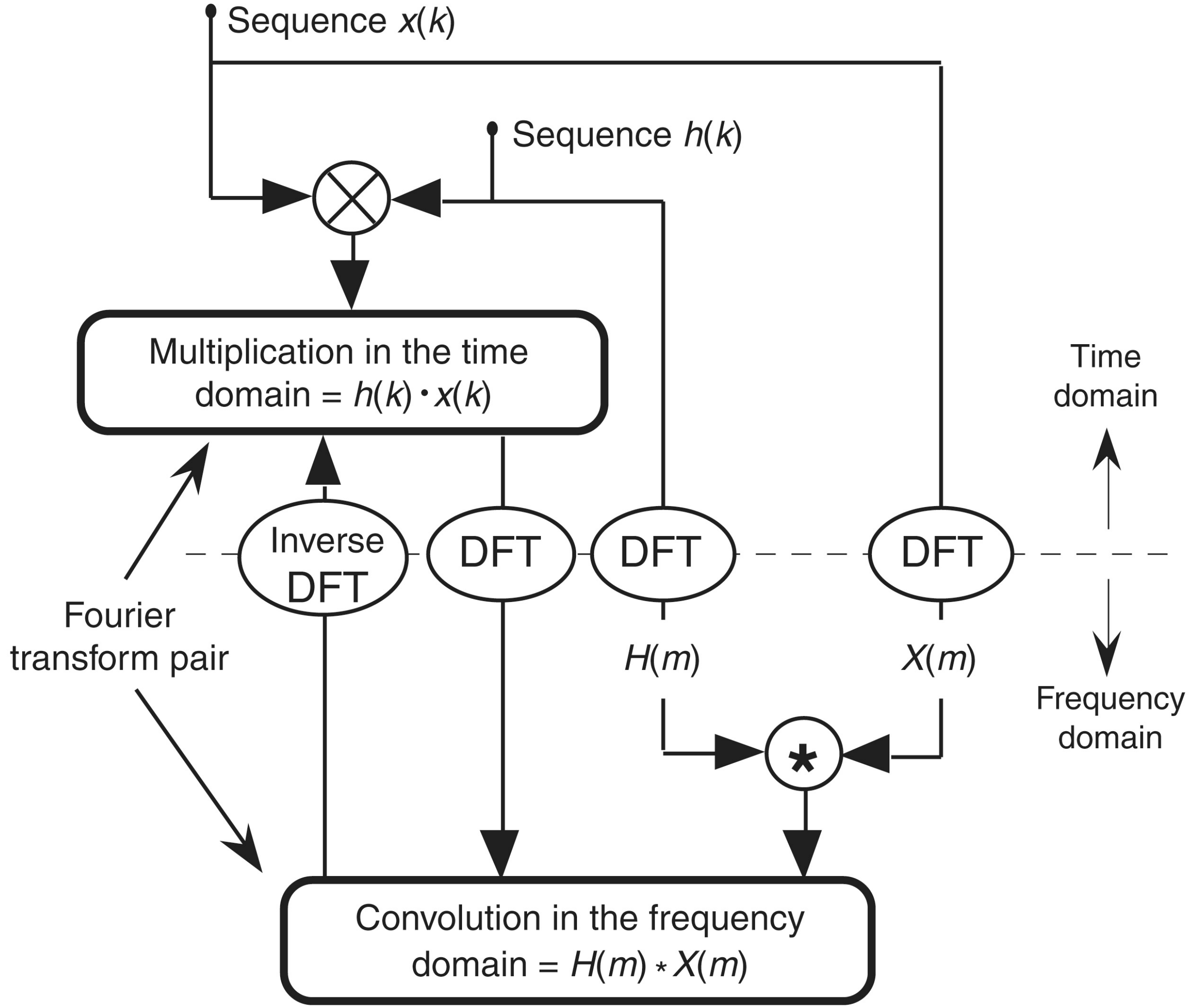

Figure 5–43 Relationships of the convolution theorem related to multiplication in the time domain.

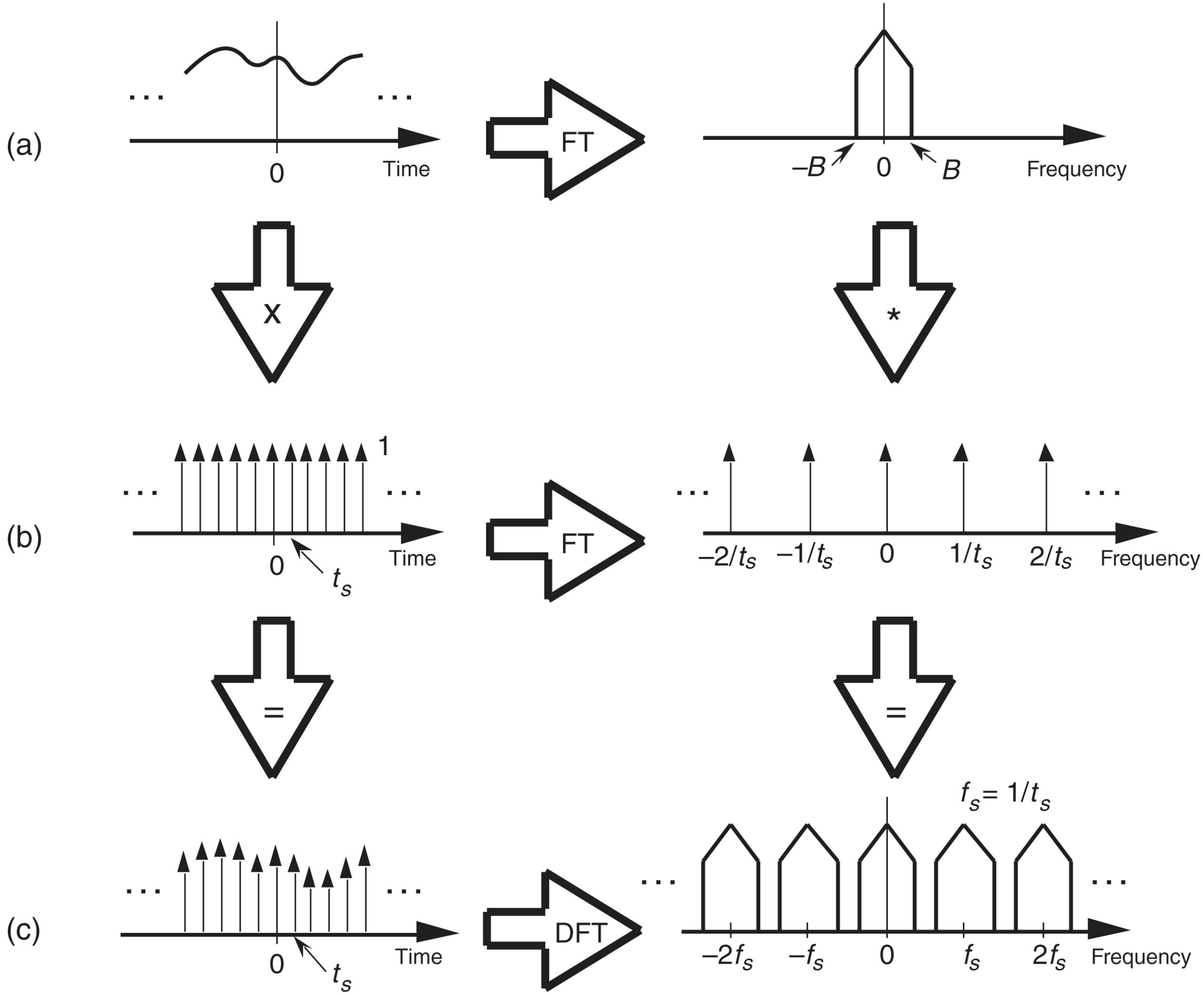

Figure 5–44 Using convolution to predict the spectral replication effects of periodic sampling.

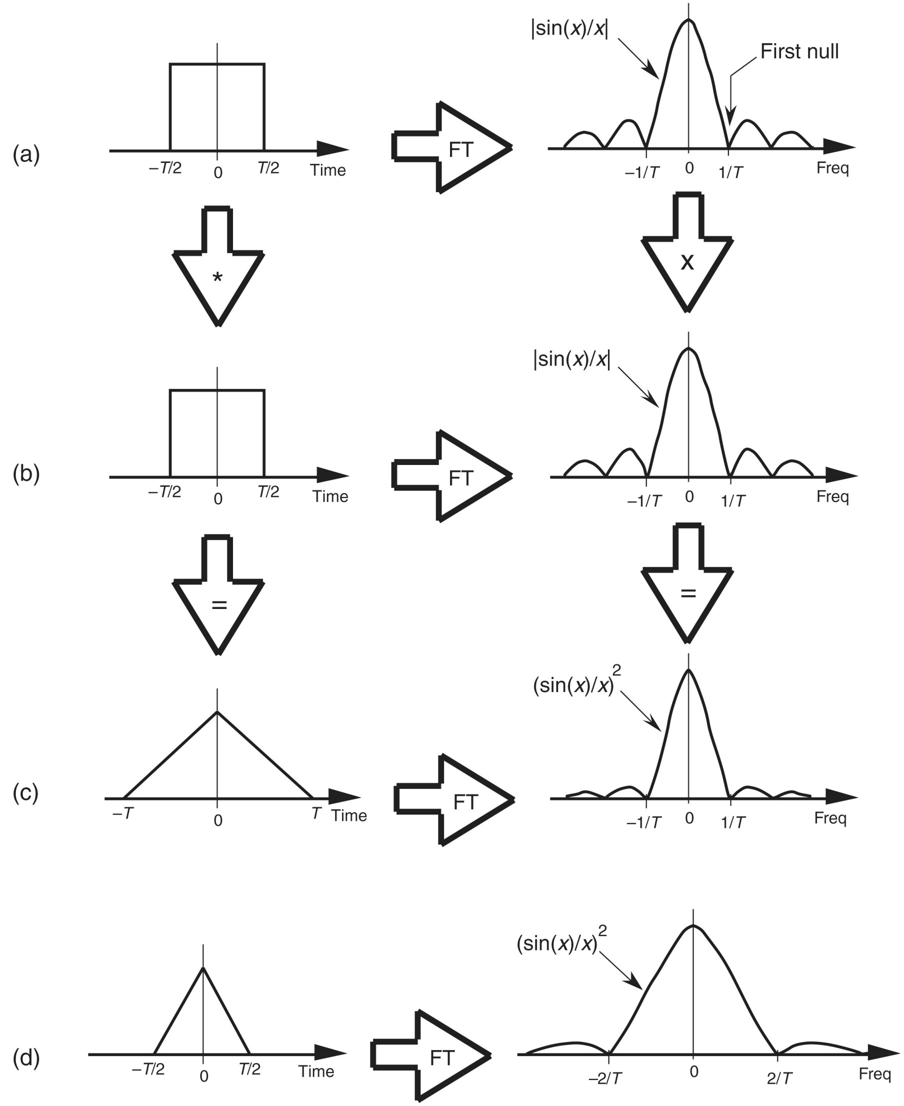

Figure 5–45 Using convolution to show that the Fourier transform of a triangular function has its first null at twice the frequency of the Fourier transform of a rectangular function.

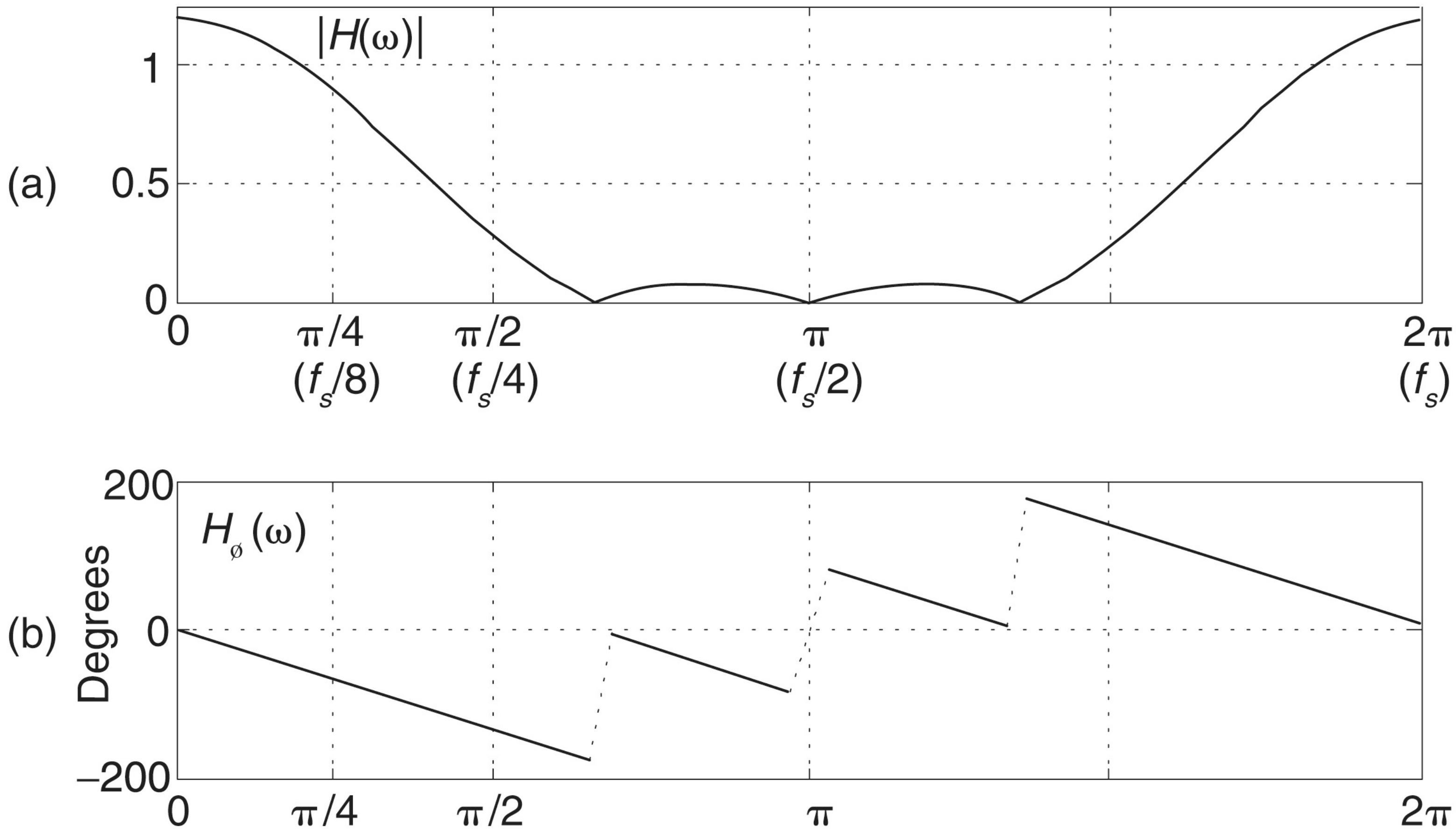

Figure 5–46 FIR filter frequency response: (a) magnitude; (b) phase.

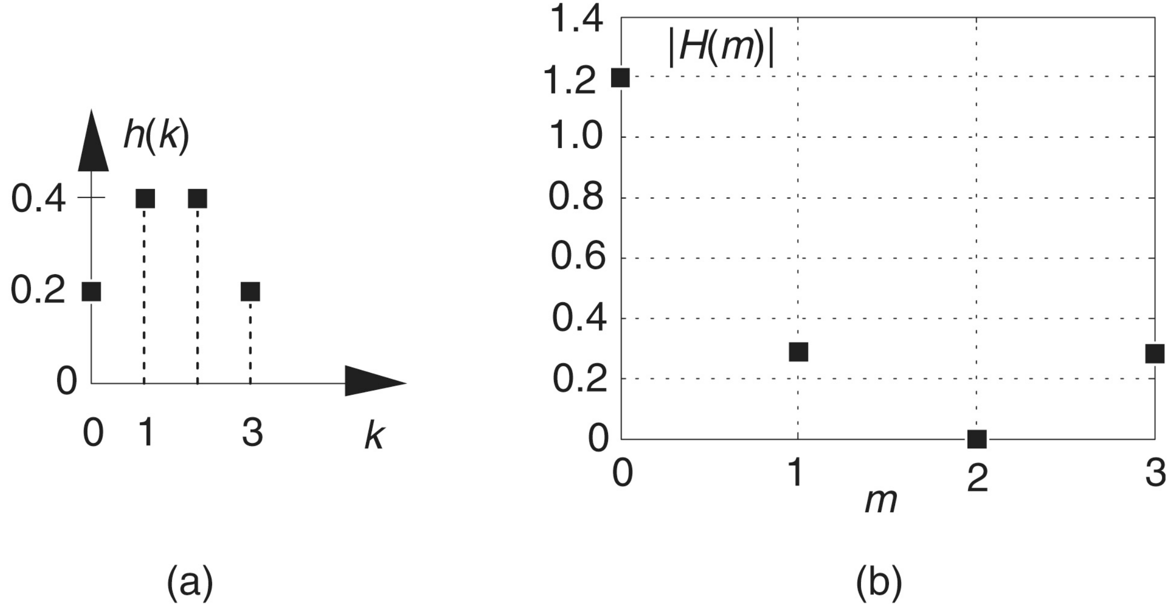

Figure 5–47 Four-tap FIR filter: (a) impulse response; (b) 4-point DFT frequency magnitude response.

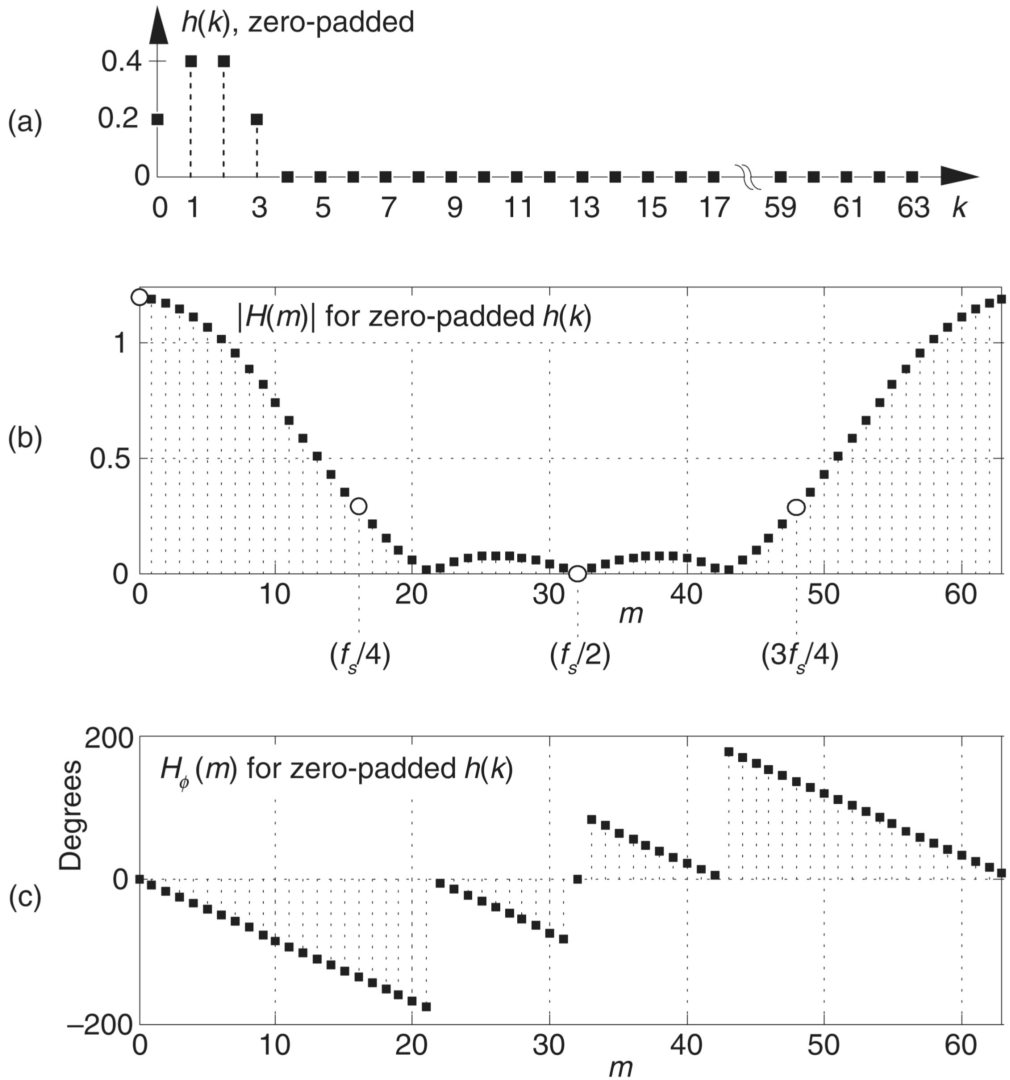

Figure 5–48 High-resolution FIR filter frequency response: (a) zero-padded *h(k)*; (b) discrete magnitude response; (c) phase response.

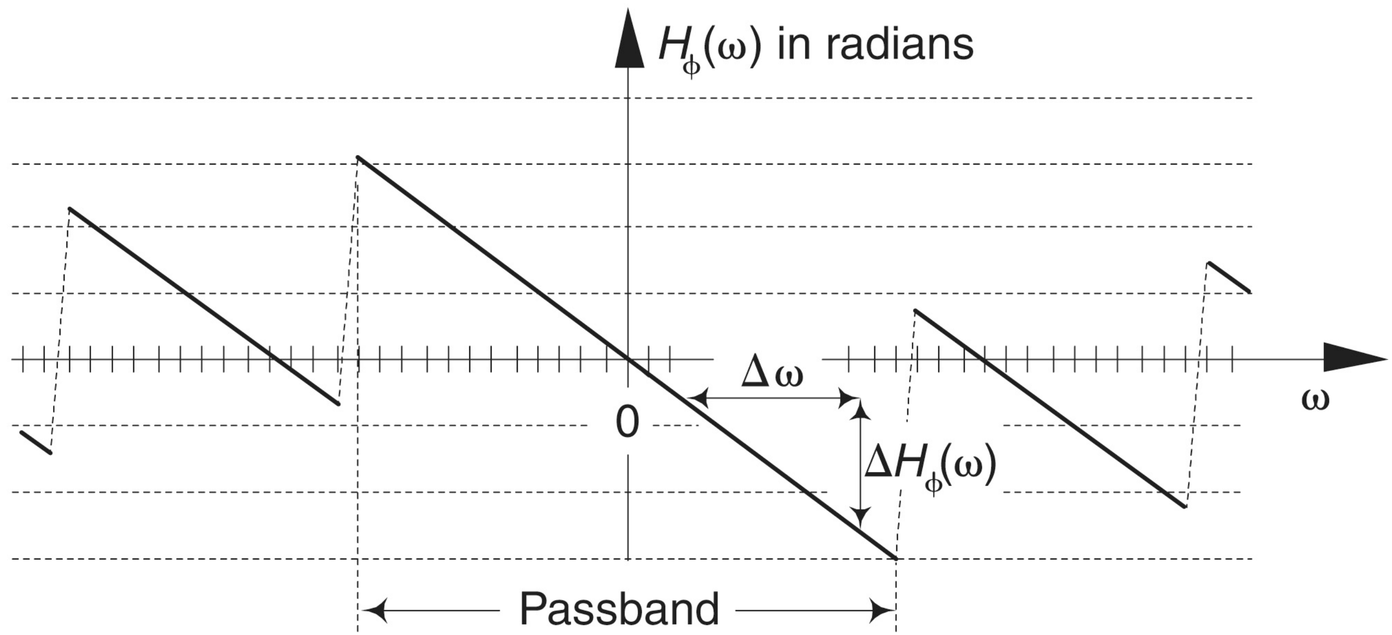

Figure 5–49 FIR filter group delay derived from a filter's phase response.

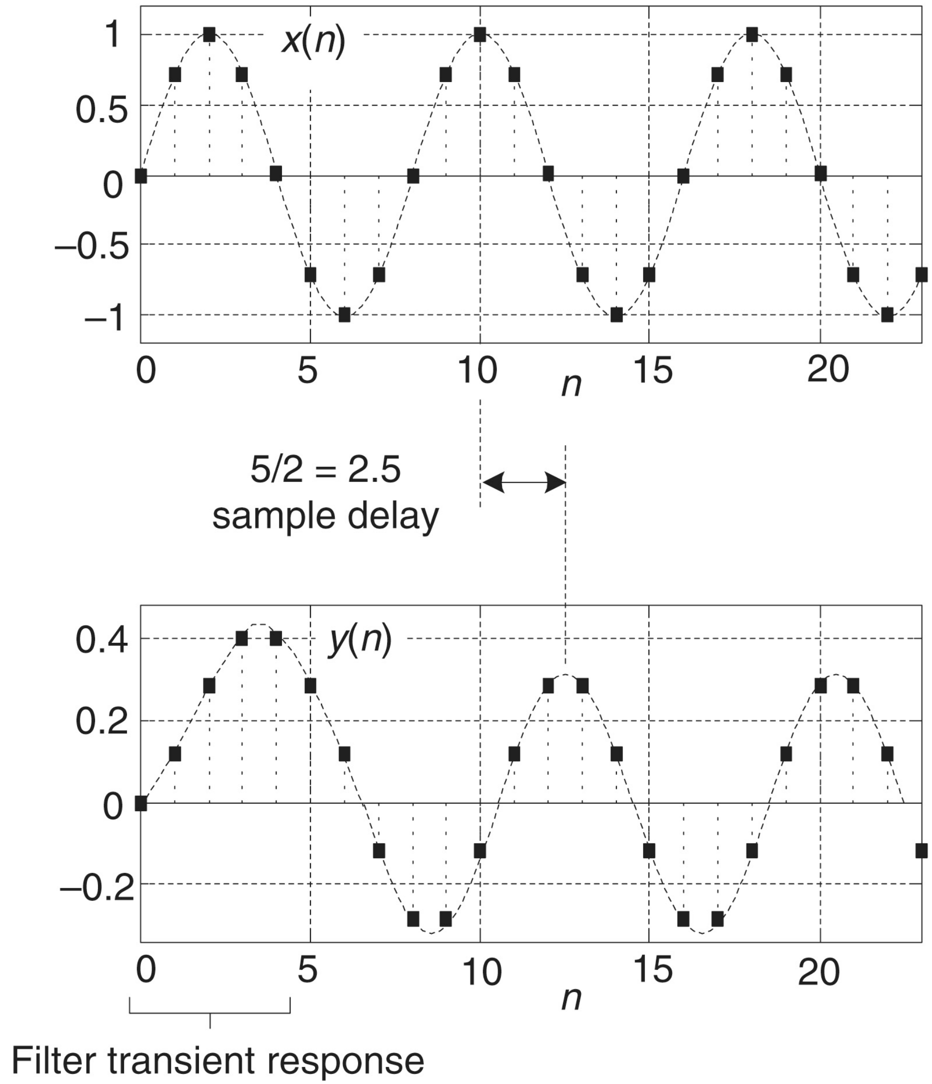

Figure 5–50 Group delay of a 6-tap (5 delay elements) FIR filter.

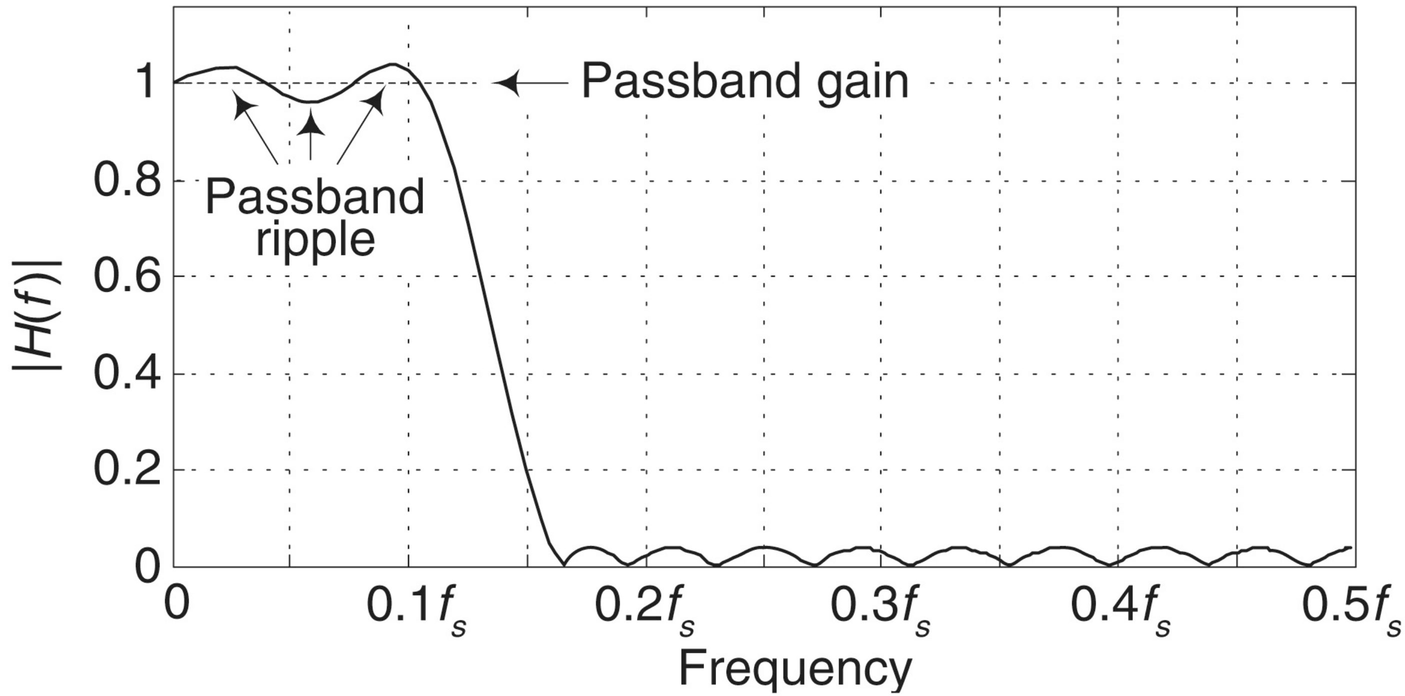

Figure 5–51 FIR filter passband gain definition.

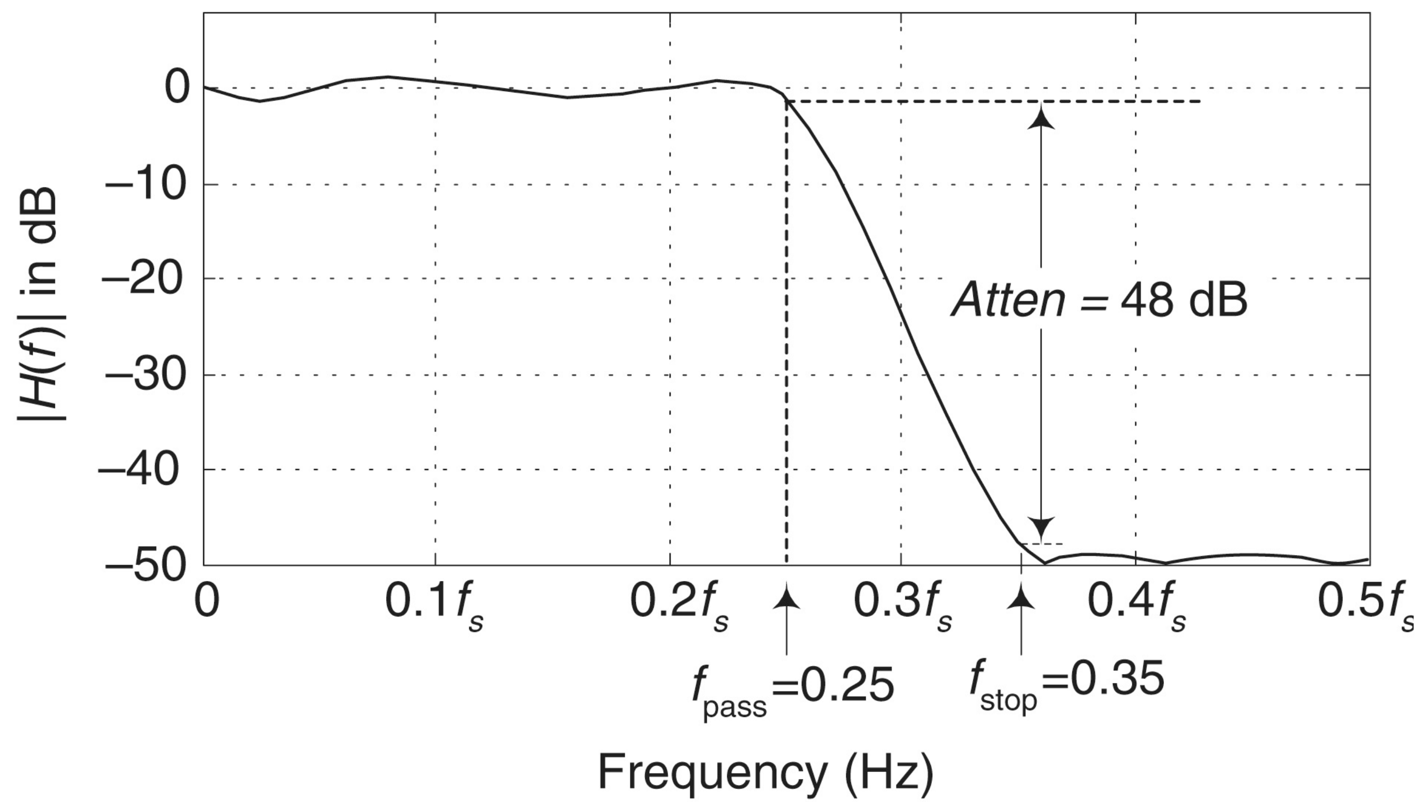

Figure 5–52 Example FIR filter frequency definitions.